3-31-2004

Light Quality And Phytoplankton Viability

Lisa A. Malick
University of South Florida

Light Quality And Phytoplankton Viability

by

Lisa A. Malick

A thesis submitted in partial fulfillment
of the requirements for the degree of
Master of Science
College of Marine Science
University of South Florida

Major Professor: Kendall L. Carder, Ph.D.
Gabriel A. Vargo, Ph.D.
John J. Walsh, Ph.D.

Date of Approval:
March 31, 2004

Keywords: photosynthesis, quantum yield, pigment, colored dissolved organic matter, absorbed radiation by phytoplankton

DEDICATION

To the one who designs and weaves the tapestry, but only allows us to see how a few threads are woven together.

ACKNOWLEDGEMENTS

Karenia brevis cell counts presented in this thesis were kindly provided by Dr. Gabriel Vargo. His research group, led by Dr. Cindy Heil, generously provided our group with ship space and oftentimes patiently waited while we collected our shipboard data. High performance liquid chromatography samples were processed by Brad Pederson and Barb Berg (Mote Marine Laboratory, Sarasota, FL) under the supervision of Dr. Gary Kirkpatrick. Financial support for this work was provided by NASA (NAS5-31716) and ONR (N00014-97-1-0006 and N00014-96-1-5013) funding. I would especially like to Dr. Kendall Carder for his constant support and guidance, and Jennifer Cannizzaro for her many hours of assistance in technical and intellectual matters.

TABLE OF CONTENTS

LIST OF TABLES

LIST OF FIGURES

Light Quality And Phytoplankton Viability

Lisa A. Malick

ABSTRACT

A method is presented, using calculations of the underwater light field, to examine viability of phytoplankton at depth. For this study, viability is defined as the ability of phytoplankton to harvest, and efficiently convert enough photons into primary production to overcome metabolic demands. How the available light field influences the production environment is examined. Changes in water column constituents, such as chlorophyll and colored dissolved organic matter (CDOM) concentration, alter the spectral quality and quantity of the light field at depth. Certain species with specialized survival strategies, such as assemblages of photoprotective and light-harvesting accessory pigments, may be better-suited to 'making a living' at depth in response to the spectral quality of the underwater light field.

Stations for study were identified from various cruises off the West Florida Shelf that exhibited variations in chlorophyll and/or CDOM concentration, including an optically complex, red-tide station. Optical and water column constituent measurements from these stations were used to develop input parameters to Hydrolight 4.1, a radiative transfer theory model, to simulate the underwater light field and to calculate absorbed radiation by phytoplankton (ARP). Values for respiration and quantum yield from the literature were used to calculate comparative values of net photosynthesis at these

stations. The effect of differences in spectral light harvesting (pigmentation), photosynthetic efficiency rates, and respiration, on viability through the water column was examined.

1. INTRODUCTION

This study focused on groups of phytoplankton living in low-light, near-bottom conditions. It examines the compatibility of their pigments with the wavelengths of available light that remain at depth, and the importance of this match to their viability. It is hypothesized that the available light field will influence the production environment under low-light, near-bottom conditions. In this study, "viability" of phytoplankton will refer to the ability of phytoplankton to harvest, and efficiently convert enough photons into primary production to overcome metabolic demands. Therefore, for the purposes of this study a phytoplankton would be "viable" above its compensation point (a depth or irradiance value at which phytoplankton exhibit zero net photosynthesis (Kirk 1994). The ability of different coastal phytoplankton taxa to harvest available light below various water-column conditions at low light levels is examined.

The depth to which a particular species remains viable, depends not only on the quantity of light available at depth, but the spectral quality. The particular pigment suite available to a species may allow that species to take full advantage of the changes in the light field with depth. Net production depends upon several factors: the quantity and quality of available light, and the ability by the phytoplankton to harvest the available wavelengths. If the absorption properties of a phytoplankton's pigments are not well-matched to the available wavelengths, that phytoplankton will harvest less light than a phytoplankton with pigments that are more compatible with the available irradiance

spectra. It is also affected by the quantum yield of photosynthesis (ϕ) and the respiration rate of the phytoplankton. Quantum yield is the efficiency with which absorbed light energy is converted to chemical energy through photosynthesis (Kirk 1994). Species with pigment suites that are well-matched to the available light field should have a competitive advantage in low-light conditions over those that do not. However, quantum yield and respiration may be more important in determining which groups out-compete the others.

In this study, optical and hydrographic data from stations in the Gulf of Mexico (GOM) are used to model the underwater light field and calculate absorbed radiation by phytoplankton (ARP) for different phytoplankton groups under various water column conditions. Stations included a dense *Karenia brevis* bloom, a nearshore cyanophyte-dominated station, and an offshore, oligotrophic station. Near-bottom simulations examine how phytoplankton with different pigment suites might compare against each other under the same lighting conditions. Literature values of quantum yield and respiration are used to estimate comparative values of net photosynthesis in simulated competitions between phytoplankton groups. However, because quantum yield and respiration can be highly variable quantities, estimations of net photosynthesis are merely for comparative purposes.

There are caveats for this study. This is solely a study of optical niches; nutrients and grazing dynamics affecting net production and population dynamics are not considered in this viability competition. Also, photons absorbed by photoprotective pigments, which do not contribute to photosynthesis, are not separated from light harvesting pigments. Therefore the absorption by phytoplankton may include photons that do not get converted

to photosynthetic product. However, this study focuses on the near-bottom, low-light environment where photoprotection is less significant.

The data used in this study were collected during Ecology and Oceanography of Harmful Algal Blooms (ECOHAB) cruises that were intended as rapid, quasi-synoptic, hydrograhic surveys of the West Florida Shelf (WFS). Collection of optical data was not the focus of ECOHAB. Therefore, no underwater irradiance measurements or other intensive optical data were collected. This study demonstrates the potential for extracting information about the water column and the optical niche it represents, from a minimal amount of optical data (above-water Rrs and the optics derived from water samples).

2. BACKGROUND

Water itself and water column constituents such as phytoplankton, colored dissolved organic matter (CDOM) and detritus are fundamental variables that determine the nature of the irradiance field as it penetrates the water column (Kirk 1994).Variations in these constituents determine the quantity and spectral quality of light through the water column. For example, CDOM absorbs strongly at the blue end of the visible spectrum, while pure water absorbs strongly at the red end of the visible spectrum. Incident light passing through a water column containing large amounts of CDOM will be rapidly depleted at the blue and red ends of the spectrum, allowing only green light to penetrate to depth. The depth to which a species of phytoplankton remains viable may largely depend upon its ability to harvest light at the wavelengths available at depth.

There are numerous examples in the literature of the influence of water composition and the resulting spectral quality of light on production at depth. Laws et al. (1990) measured primary production and pigment concentrations in the North Pacific Tropical Gyre. They demonstrated that primary production rates can be underestimated by about a factor of two if incubations are not conducted under light conditions that reflect the spectral characteristics of the underwater light field. Farmer et al. (1993) measured the underwater light field in the eastern Caribbean Sea during a period of high Orinoco River flow. The authors found that the spectrum of light (at a depth of 5 m) shifted to longer

wavelengths. In a related study, Bidigare et al. (1993) noted that the phytoplankton population had shifted to species containing pigments which absorb at these longer wavelengths, providing evidence that the Orinoco River modifies both the vertical distribution and composition of Caribbean phytoplankton during periods of high outflow. Bidigare et al. (1987) estimated primary productivity using a spectrally dependent bio-optical model based upon measurements of spectral quantum irradiance as a function of depth, concentrations and specific absorption coefficients of the major pigment groups, and quantum yield of photosynthesis. The authors noted the paucity of *in situ* determinations of absorbed radiation by phytoplankton (ARP) for natural phytoplankton populations (see Section 3.3 for a definition of ARP). They argue that these data could provide insight into how phytoplankton utilize the light field with depth, how optical properties of the water column are influenced by phytoplankton, and how phytoplankton populations are partitioned in space and time. The study presented here describes a method for modeling ARP for natural phytoplankton populations and attempts to address these questions.

3. METHODS

Figure 1 provides an overview of the methods employed in this study. Field data from two ECOHAB cruises (Figure 2) on the West Florida Shelf (WFS) were used as input to Hydrolight 4.1, a radiative transfer theory model (Mobley 1994), to estimate the

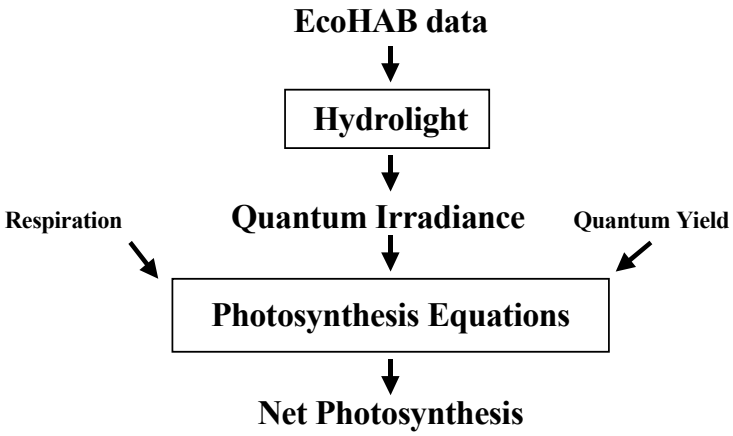

Figure 1. Overview of Methods

underwater light field and calculate Absorbed Radiation by Phytoplankton (ARP). Dark respiration and quantum yield values from the literature (Bidigare et al. 1989; Henley and Yin 1998; Shanley 1985) were used with ARP (see section 3.3) to calculate comparative values for net photosynthesis of phytoplankton through the water column. Comparisons

are made of ARP and net photosynthesis, as model parameters such as the absorption properties of the resident phytoplankton, irradiance level, and the nature of quantum yield are varied. Various phytoplankton groups with different absorption properties then compete for photons and utilize them under various water-column conditions based on model conditions.

3.1 ECOHAB data

Surface seawater samples were collected with an eight-liter Niskin bottle or a bucket for analysis. Samples were filtered immediately following collection. Filters were stored in liquid nitrogen for no more than one week prior to processing. Particulate and detrital absorption spectra were determined using the quantitative filter technique (Kiefer and Soohoo 1982; Yentsch 1962). Absorption spectra were measured using a custom-made, 512-channel spectroradiometer (350-850 nm) based on the methodologies discussed in Carder et al. (1999). Chlorophyll concentrations were determined fluorometrically (Holm-Hansen 1978). For absorption spectra of CDOM, 0.2 μm filtrates were stored at –30^{o}C for less than three weeks, thawed slowly, and refiltered prior to processing. Milli Q water was used as a reference and samples were scanned in 10 cm cells using a Perkin-Elmer Lambda 18 spectrophotometer.

Conductivity-temperature-depth (CTD) profiles providing salinity, temperature, chlorophyll fluorescence, and sigma theta with depth were made at each station. Surface attenuation, backscattering and chlorophyll fluorescence were measured using an underway surface flow-through system. Seawater from approximately 2 m depth was pumped by the ship's flow-through system into a 0.5 m^3 optically black chamber

equipped with a CTD (Falmouth-Scientific), chlorophyll fluorometer (WetLabs), CDOM fluorometer (WetLabs), and a Hydroscat-2 backscattering meter (HOBI Labs). The backscatter coefficient at 550 nm was estimated by fitting a spectral power function to the measured wavebands at 488 nm and 676 nm, then interpolating to 550 nm. Particulate backscattering, b_{bp}, was then calculated by subtracting backscattering due to water (Morel 1974).

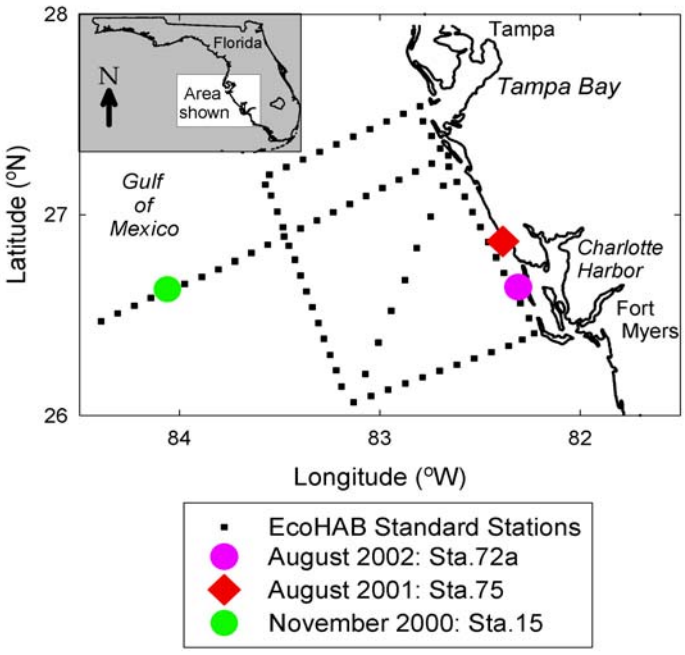

Figure 2. Study Area West Florida Shelf ECOHAB

Hyperspectral R_{rs} measurements were collected from above the water during daylight hours using a custom made, hand-held 512-channel spectroradiometer equipped with a 10^{o} field-of-view. Data collection and processing are described in Lee et al. (1996).

3.2 Hydrolight 4.1

Hydrolight 4.1 is a numerical model of radiative transfer. It computes radiance distributions and related quantities (irradiances, reflectances, diffuse attenuation functions, etc.) in the ocean. In a comparison with six other radiative transfer models, all models, including Hydrolight, were found to compute irradiance with the same or greater accuracy as measured values (Mobley et al. 1993). Hydrolight was chosen for this study because of its computational efficiency and user-friendly, graphic user interface. In this study, absorption and scattering properties of the water column constituents, sky conditions, and bottom boundary conditions obtained from ECOHAB station data and cruise notes were used as input to this model. Based on this input, Hydrolight computes the in-water light field, remote-sensing reflectance, and other quantities of interest to optical oceanographers. The quantities of interest for this study are the underwater quantum scalar irradiance distribution ($E_o(\lambda, z)$), which is used to estimate $ARP(\lambda, z)$, and the in-air remote-sensing reflectance (R_{rs}), which is compared against measured values of R_{rs} for model validation. Details of the input to Hydrolight at each station are given in the appropriate chapter for each station.

3.3 Photosynthesis calculations

Kirk (1994) provides a simple model of photosynthesis based on available light, the phytoplankton absorption coefficient, and quantum yield of photosynthesis. Using the Hydrolight-generated depth profiles of quantum scalar irradiance ($E_o(\lambda, z)$), depth profiles of Absorbed Radiation by Phytoplankton ($ARP(\lambda, z)$) are calculated:

$$ARP(\lambda, z) = E_0(\lambda, z) * a_{phi}(\lambda, z) \quad (1)$$

where a_{phi} is the absorption coefficient due to phytoplankton. It is determined by subtracting the measured absorption due to detritus from that of particles. As the product of quantum scalar irradiance and the phytoplankton absorption coefficient, ARP is a measure of the available light that a phytoplankton is capable of harvesting. ARP is the spectral counterpart to Photosynthetically Utilizable Radiation (PUR), while E_o is the spectral counterpart to Photosynthetically Available Radiation (PAR)(Smith and Baker 1981). Both PUR and PAR are broadband quantities (integrated across the visible spectrum) while E_o and ARP are spectral quantities.

Once ARP is calculated for the water column, values for quantum yield of photosynthesis and dark respiration (R_d) from the literature were used to estimate comparative values of net photosynthesis (P_{net}) throughout the water column for the various simulations, according to the equations:

$$P_{gross}(z) = \phi \int_{400}^{700} ARP(\lambda, z) d\lambda \quad (2)$$

$$P_{net}(z) = P_{gross}(z) - R_d(z) \quad (3)$$

The effect of variations in the absorption properties on ARP and P_{net} with depth, that were due to changes in pigment absorption, was evaluated.

3.4 ECOHAB Station 72a (August 2002)

3.4.1 Station description

Station 72a is a nearshore station, close to Charlotte Harbor (26.64°N, 82.31°W). Data were collected by the R/V Suncoaster at 1715 hrs (local time). Water depth was 11 m. Surface and 8 m samples were taken for absorption and chlorophyll concentration measurements. CTD profiles in Figure 3 indicate an upper layer of warmer, lower-salinity, higher-chlorophyll water. At about 4-5 m there is a transition to a well-mixed subsurface layer.

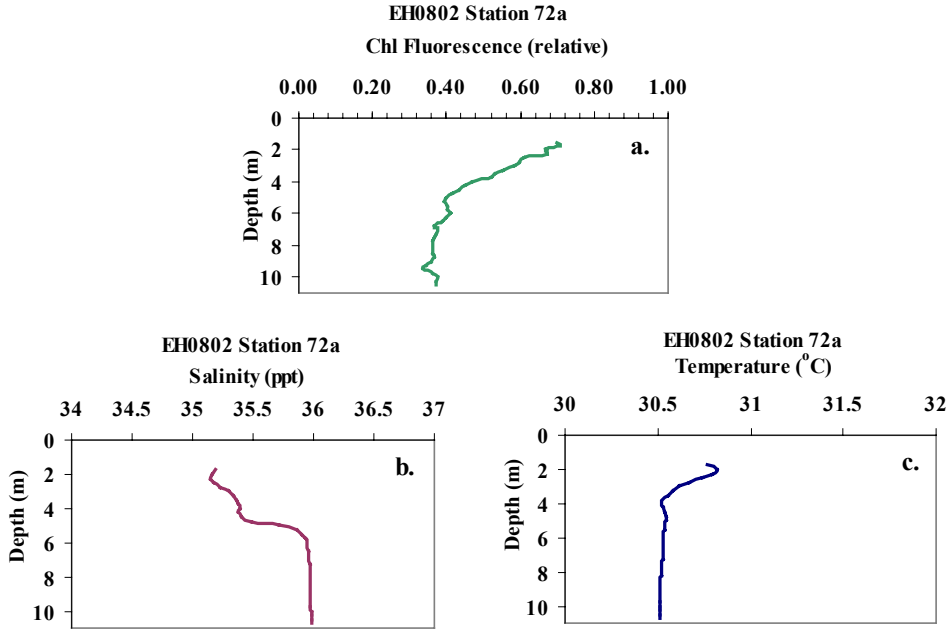

Figure 3. EH0802 Station 72a: CTD profiles of a.) chlorophyll fluorescence b.) salinity c.) temperature.

This station was chosen for an interesting characteristic in the phytoplankton absorption spectra (Fig 4). In addition to the typical chl *a* absorption peaks at about 438 nm and 675 nm, both spectra exhibited a small but distinct peak, centered at about 548 nm. This peak is indicative of phycoerythrobilin (PE), a water-soluble, light-harvesting phycobiliprotein, found in cyanophytes, cryptophytes and to a lesser extent rhodophytes. Also, note a shoulder from about 455 nm - 495 nm which may indicate the presence of a second phycobiliprotein, phycourobilin (absorption peak about 495nm) as well as, zeaxanthin and other photoprotective carotenoids (absorption peaks about 455nm - 475nm) (Jeffrey et al. 1997; Morel 1997).

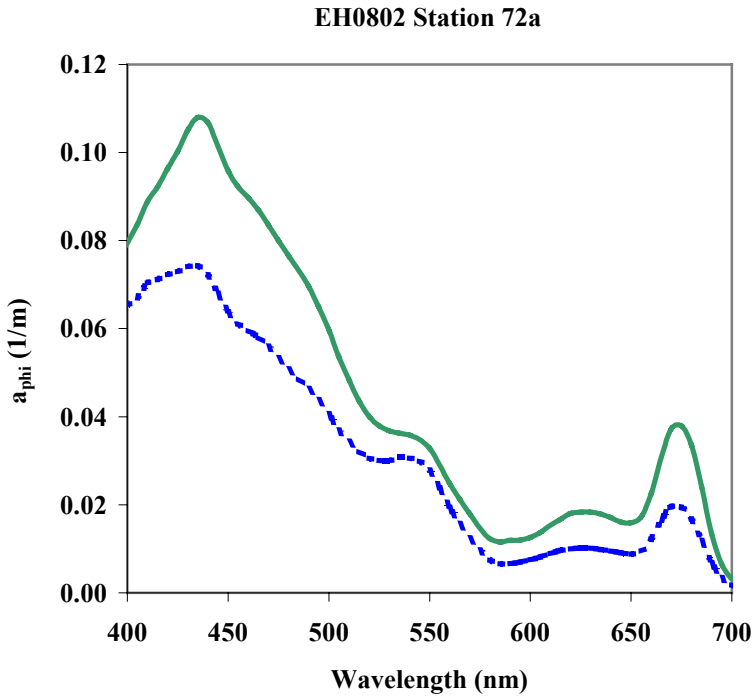

Figure 4. EH0802 Station 72a: Measured phytoplankton absorption spectra at surface (solid line) and 8 m (dashed line)

In order to select respiration rates and values for quantum yield of photosynthesis from the literature, it was necessary to make some simplifying assumptions about the phytoplankton composition at this and the other sites of interest. Neither cell counts nor HPLC analysis of pigments were available for Station 72a; therefore more indirect evidence was used to select a representative species for this station. The presence of absorption peaks for the pigments, phycoerythrobilin, phycourobilin, and zeaxanthin are not exclusive to cyanophytes; they are also found in cryptophytes and to a lesser extent rhodophytes (Jeffrey et al. 1997; Morel 1997). However, cruise notes reported pink staining of the filter pad (present before and after MEOH extraction), which can indicate a large number of cyanophytes, such as *Synechococcus* or *Trichodesmium* (Jeffrey et al. 1997; Morel 1997). Cruise notes also reported a *Synechococcus* bloom at the mouth of the Caloosahatchee River, just south of this station. Therefore, for the purpose of selecting a respiration rate and quantum yield values, *Synechococcus* was chosen as the representative species for Station 72a

Cyanophytes	**Major (Minor)**	
Major Pigments	**Abs Peaks (nm)**	**Function**
Chl a	**430, (662)**	**LH**
Phycoerythrobilin	**548**	**LH**
Phycourobilin	**495**	**LH**
Phycocyanin	**610**	**LH**
Allophycocyanin	**650**	**LH**
Zeaxanthin	**(428), 454, 481**	**LH/PP**

Table 1. Major pigments in cyanophytes (Jeffrey 1980; Jeffrey et al. 1997; Morel 1997). Absorption peaks are in acetone solvent. LH: Light-Harvesting, PP: Photoprotective.

3.4.2 Hydrolight simulations

The depth profiles for chlorophyll concentration and the chlorophyll specific absorption coefficient were derived from the relationship between the measured chlorophyll fluorescence profile and the two measurements (at the surface and 8 m) of chlorophyll concentration and absorption. The depth profile for $a_{CDOM}(420)$ was determined by linearly interpolating the measured $a_{CDOM}(420)$ at the surface and 8 m against the salinity downcast.

Backscattering efficiency (b_b/b): The scattering coefficient ($b(\lambda)$) can be determined by subtracting the total absorption coefficient at each wavelength (λ) from the total attenuation coefficient, according to the equation:

$$b(\lambda) = c(\lambda) - a_{TOT}(\lambda) \quad (4)$$

where a_{TOT} is the sum of the absorption coefficients for particles, CDOM and water. ($a_{TOT}(\lambda) = a_p(\lambda) + a_{CDOM}(\lambda) + a_w(\lambda)$). The scattering coefficient at 480 nm, b(480), was determined from surface measurements of c(480), $a_p(480)$, and $a_{CDOM}(480)$. The absorption coefficient due to water is known (Pope and Fry 1997). Backscattering at 480 nm, $b_b(480)$, was estimated from measured values of $b_b(488)$ and $b_b(676)$ using a spectral power function. Thus, a backscattering efficiency was calculated from $b_b(480)/b(480)$. A summary of the inputs to Hydrolight 4.1 for this study can be found in Appendix A. Hydrolight results were validated by comparing modeled and measured remote sensing reflectance (R_{rs}).

A second Hydrolight run was made for Station 72a, using the same inputs except that the phycoerythrobilin (PE) peak was removed from the phytoplankton absorption curve. The purpose of this second Hydrolight run was to examine how removal of this

major, light-harvesting pigment changes the modeled ARP. This will affect P_{net} calculations with depth, and may make a difference in the depth to which this species remains viable. Results from this "No PE" peak Hydrolight simulation were compared with those for the initial "w/PE" peak simulation. Figure 5 shows the chlorophyll-specific absorption (a^*_{phi}) curve for Station 72a with and without the PE peak. Chlorophyll-specific absorption is the absorption due to phytoplankton per unit chlorophyll.

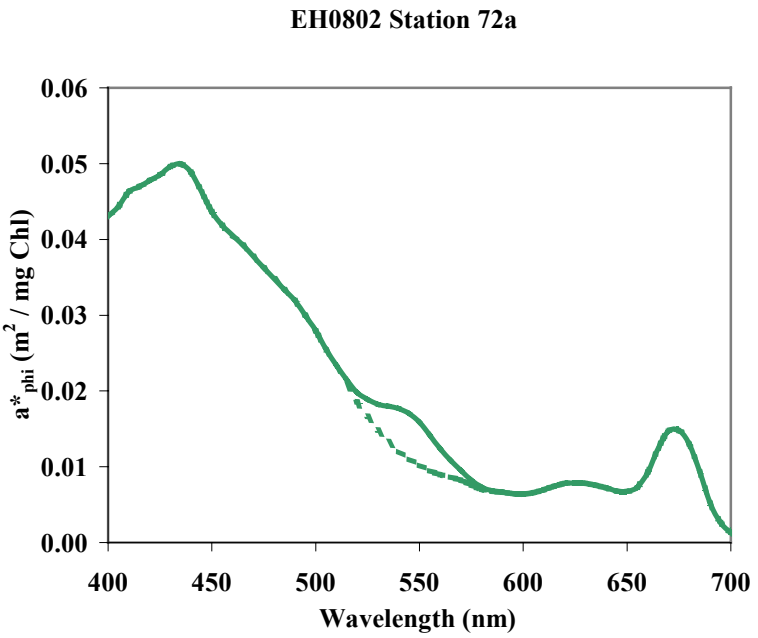

Figure 5. EH0802 Station 72a: Chlorophyll specific absorption curves for the phytoplankton component of the Hydrolight model. The dashed line shows a^*_{phi} with the 548 nm phycoerythrobilin peak removed.

3.5 ECOHAB Station 75 (August 2001)

3.5.1 Station description

Station 75 is a nearshore station north of Charlotte Harbor (26.87°N, 82.39°W). Data were collected by the R/V Bellows at 1705 hrs. (local time). Water depth was 8.3 m. A very large *K. brevis* bloom was present (Cell count: 7 million cells L^{-1}, chl *a* concentration: 130 mg m^{-3}).

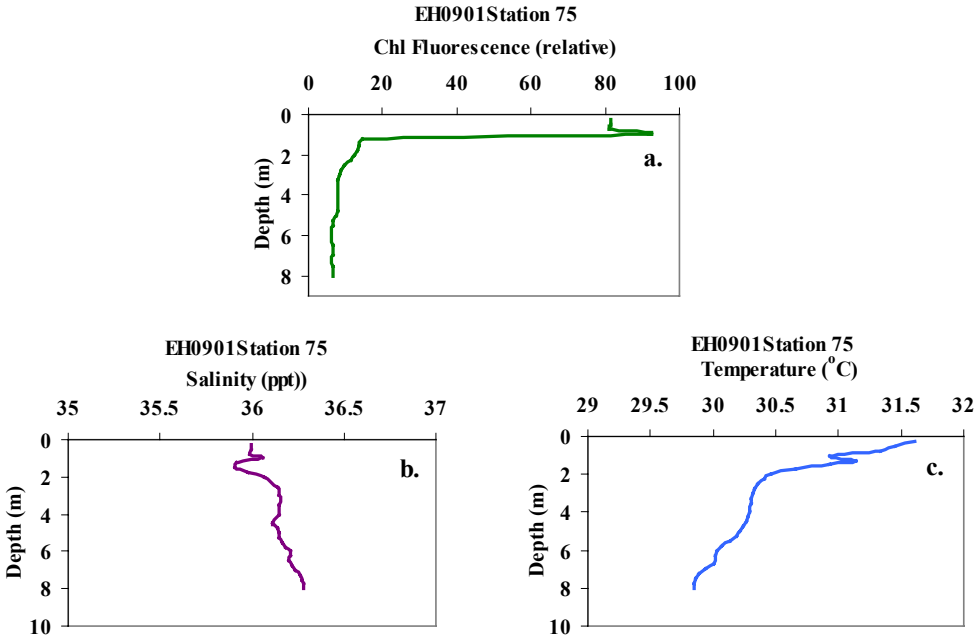

Figure 6. EH0901 Station 75: CTD profiles of a.) chlorophyll fluorescence b.) salinity c. temperature.

Station 75 is characterized by a dense *K. brevis* bloom *and* a large CDOM plume near the surface. The high concentrations of both chlorophyll and CDOM at this station, made the water brown in appearance. The CTD profiles in Figure 6 show a transition between 1-2.5 m from a surface bloom to a relatively well-mixed, subsurface layer. Despite the high CDOM levels, the CTD profile of salinity in Figure 6b revealed relatively high salinity, indicating that the source of the CDOM is largely phytoplankton rather than terrigenous influences. In fact, the $a_{CDOM}(440):a_{phi}(440)$ ratio was 0.49, making this station effectively a Morel Case 1 station (Walsh et al. 1992). Due to the *K. brevis* bloom, the surface layer had extremely high chlorophyll fluorescence (Figure 6a). Note the sharper gradient for chlorophyll fluorescence than for salinity or temperature, suggesting that some factor (e.g. phototaxis) other than strict mixing may be operative at this station.

At Station 75, phytoplankton absorption is overwhelmingly dominated by the toxic dinoflagellate, *Karenia brevis*. In addition to cell counts of this species, HPLC analysis reveals the presence of the pigment, gyroxanthin diester at this station. This pigment is considered a biomarker for *K. brevis* (Kirkpatrick et al. 2000). Therefore, for the purpose of selecting a respiration rate and quantum yield values, the obvious choice for the representative species for this station was *K. brevis*.

3.5.2 Optimization model

Station 75 represents an optically complex, two-layer system, requiring a more sophisticated approach to modeling the required input parameters for Hydrolight. Because only surface absorption values were measured on the R/V Bellows at this

station, input values for two individual layers were first estimated using the optimization model of Lee et al. (1999a). The Lee model is a hyperspectral R_{rs} model for shallow water, in which a remote-sensing reflectance spectrum is modeled from a set of values of absorption, backscattering, bottom albedo, and bottom depth. The modeled and measured R_{rs} spectra are compared. Then, the difference between the two spectral curves is minimized and the set of variables optimized, by adjusting the model values in a predictor-corrector scheme. In this way, absorption coefficients, bottom depths, and other properties can be derived simultaneously. Full details are given in Lee et al. (1999b). In this study, instead of modeling bottom reflectance, this algorithm was used to model an optically unique, second layer of the water column with reduced chlorophyll and CDOM.

3.5.3 Addition of gaussian curves to phytoplankton absorption spectra

Gaussian shapes can be used to represent the absorption spectra of individual photosynthetic components (Hoepffner and Sathyendranath 1991). In order to adequately match the measured R_{rs} curve for this station, two gaussian curves at 590 nm and 635 nm were added to the measured phytoplankton absorption curve. The peaks of these curves correlate with known chlorophyll *c* absorption peaks found in *K. brevis* (Millie et al. 1997). The parameters for these curves are shown in Table 2.

	Gauss 1	Gauss 2
Amplitude (m^{-1})	0.15	0.35
Peak wavelength (nm)	590	635
Bandwidth (nm)	20	24

Table 2. Gaussian curves added to Station 75 a_{phi}

Addition of these peaks allowed for a better fit between measured and modeled R_{rs} curves. These chlorophyll *c* absorption features may have been less pronounced at the surface where the sample for this station was taken. A deeper sample, where absorption at these longer wavelengths may become more important, may have revealed these enhanced absorption features.

Figure 7 shows the phytoplankton and CDOM absorption curves generated from the 2-layer model, including the addition of the two gaussian curves to the a_{phi} curves. Layer 1 represents the top meter of a dense *K. brevis* bloom. Layer 2, from 1 - 8.3 m, represents the well-mixed water column below the surface bloom. Absorption by phytoplankton and CDOM is much reduced for the second layer than the first.

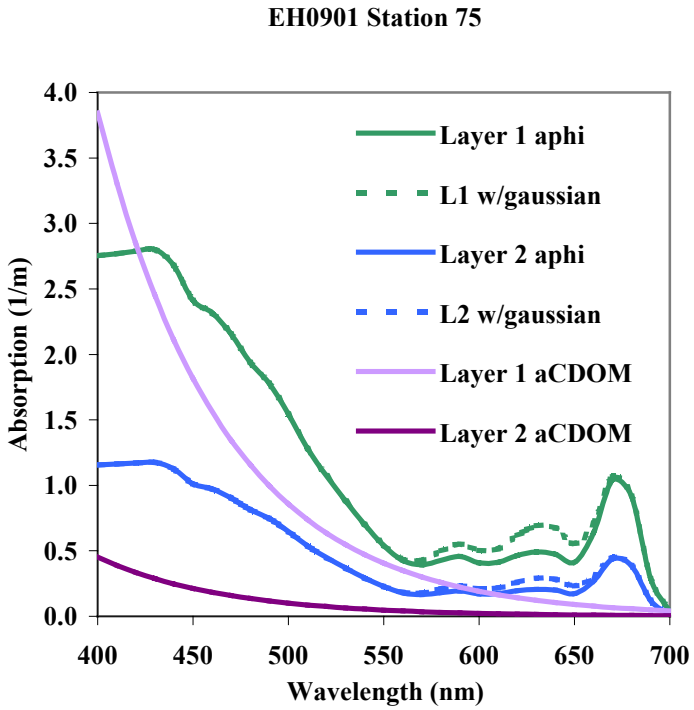

Figure 7. EH0901 Station 75: Modeled phytoplankton and CDOM absorption curves used as input to Hydrolight. Added gaussian curves are shown as dashed lines.

Figure 8 shows the results of the Lee optimization model compared against the measured R_{rs} at Station 75. The additions of the chl *c* absorption features result in a modeled R_{rs} curve that provides an excellent match with the measured R_{rs} curve, except at the 685 nm fluorescence region, which is not included in the Lee model. The backscattered contribution to R_{rs} from Layer 2 (from 1 - 8.3 m) provides most of the R_{rs} signal and gives it most of its shape. Layer 1 (the "red-tide" layer) contributes a relatively flat signal to the R_{rs}. *K. brevis* has relatively low backscattering (Cannizzaro et al. 2002) and the high concentration of cells contribute strongly to the absorption rather than the backscattering of light.

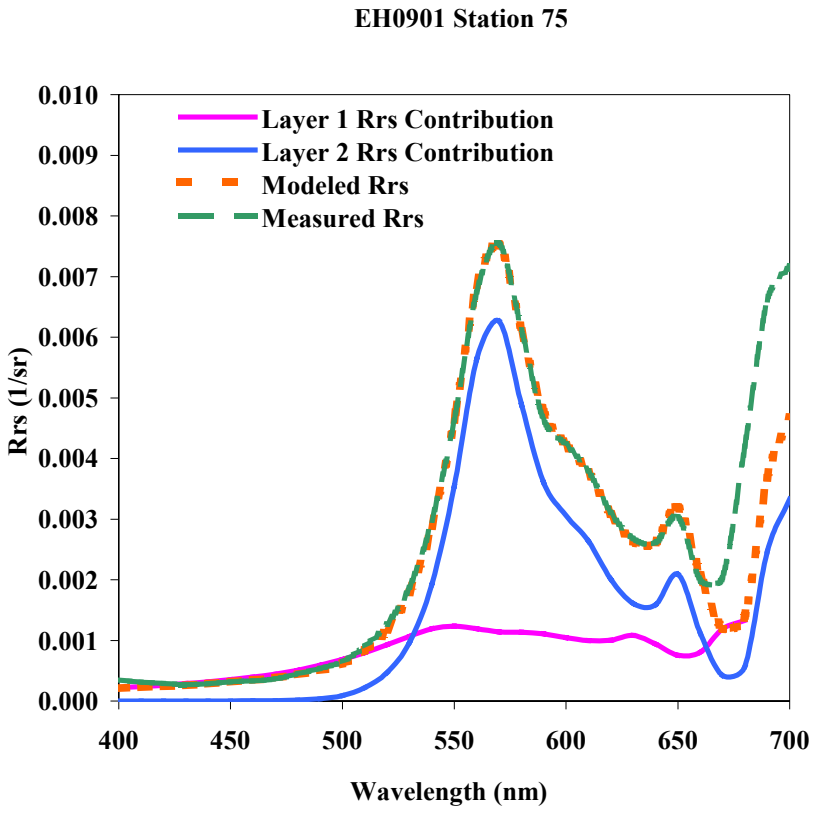

Figure 8. EH0901 Station 75: Model validation. Results of Lee's optimization model using a two-layer system, compared against measured remote sensing reflectance at Station 75.

3.5.4 Hydrolight simulations

The optimized parameters from Lee's model were used as input for a 2-layer simulation in Hydrolight. These parameters, and all inputs to Hydrolight are described in Appendix A. A second Hydrolight run was made, using all the same inputs except solar zenith angle, which was changed from 53.2^{o} to 27.51^{o}, to simulate noon irradiance conditions. The two runs will be referred to as the "5 PM " simulation and the "Noon" simulation. As with Station 72a, Hydrolight-generated depth profiles of $E_o(\lambda)$ were used to calculate depth profiles of ARP(λ). Then dark respiration and quantum yield values from the literature were used with ARP to calculate comparative values for net photosynthesis through the water column. Comparison of the two Hydrolight runs examine how much a change in incident irradiance affects ARP modeled from Hydrolight and how this will affect the depth to which this species remains viable.

3.6 Deep Comparisions

Using Hydrolight simulations of the underwater light field for both stations, some comparisons were made of net photosynthesis in the bottom meter to examine how phytoplankton with different pigment compositions would compete at these two stations. For both stations, ARP and net photosynthesis in the bottom 1 meter of the water column are compared when calculated with phytoplankton absorption curves from various representative phytoplankton or phytoplankton assemblages. These near-bottom simulations examine how phytoplankton with different pigment suites might compare against each other in light harvesting and net production, under the same water-column

conditions. Which group possesses the 'pigment suite' that can take full advantage of the changes in the light field with depth and out-compete the others is assessed.

For Station 72a, an upper layer with phytoplankton absorption with no phycoerythrin peak (Figure 5, "Station 72a No PE") was used in a simulation of the light field entering the bottom meter (from 10 - 11 m). Three comparisons were made in which the bottom meter had absorption properties from:

1. Station 72a "w/PE."
2. A winter, offshore station (described below).
3. Station 75, K.brevis bloom station.

For Station 75, the original "5 PM" Hydrolight simulation is used for the upper layer. Three comparisons were made in which the bottom meter (roughly 7.5 - 8.3 m) had absorption properties from:

1. Station 72a "w/PE" peak.
2. Station 72a "No PE Peak."
3. A winter, offshore station (described below).

Chlorophyll concentrations for the bottom meter were standardized among the groups for each station simulation, so that both ARP and photosynthesis calculations are comparable among the stations. As seen in Figure 9, the absorption curves for all groups were normalized at the red peak to provide similar chlorophyll-specific absorption curves at 675 nm. For the simulation of Station 72a, the curves were normalized to the Station 72a curve; likewise for the Station 75 simulation (not shown).

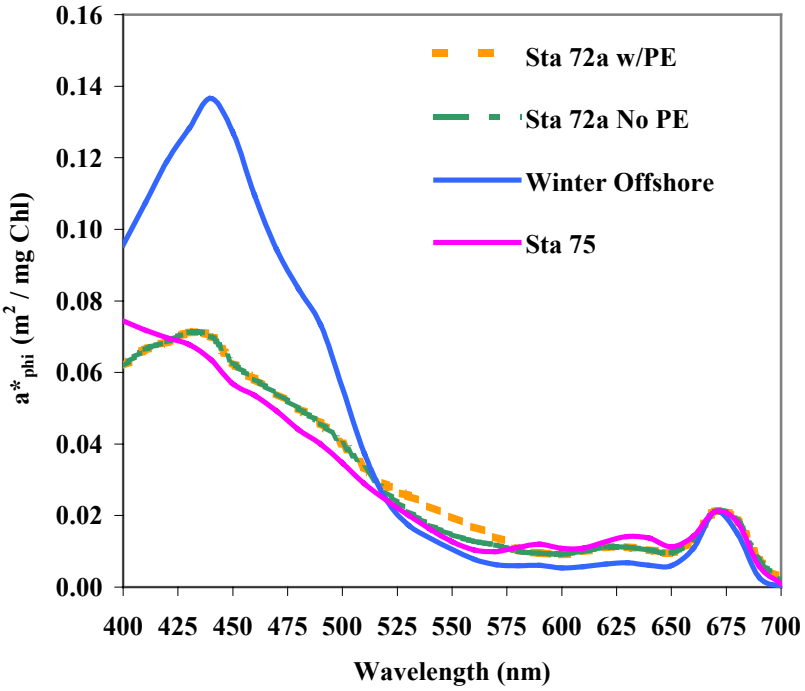

Figure 9. Chlorophyll specific phytoplankton absorption curves from various stations, representing different phytoplankton populations. Curves are normalized at the red peak to Station 72 curves.

The absorption curve for the Offshore station is from Station 15 of the November, 2000 ECOHAB cruise. This sample was taken at 26.63°N, 84.06°W, at 30 m depth. The bottom depth was 125 m, and the reported water color was blue.

Cannizzaro et al. (2002) describe three, bio-optically unique provinces on the WFS, dominated by prochlorophytes and cyanophytes, diatoms, and *K. brevis*. The authors report that HPLC data indicate that waters west of the 50 m isobath (away from terrigenous influences) were dominated by prochlorophytes and cyanophytes. Wawrik et al. (2004) also reported that offshore waters not associated with the Mississippi plume were numerically dominated by *Prochlorococcus*. HPLC analysis was not available for this station; however HPLC analysis of the neighboring station (26.63°N, 84.40°W,)

reveals high concentrations (relative to chl *a*) of divinyl chl *a* and zeaxanthin. Divinyl chl *a* is a pigment that is specific to prochlorophytes, and zeaxanthin is found in prochlorophytes and cyanophytes. HPLC analysis also revealed low relative concentrations of chlorophyll c, which is found in cryptophytes, but not cyanophytes or prochlorophytes (Jeffrey et al. 1997). This station appeared to have a mixed population, dominated by prochlorophytes.

3.7 Selection of quantum yield values

For the initial simulations for Station 72a, P_{net} was calculated using a spectral quantum yield and a non-spectral (broadband) quantum yield based on the work of Bidigare et al.(1989). The authors grew cultures of a Bermuda strain of a *Synechococcus* clone, WH7803 (DC2). They measured absorption, pigmentation, and carbon action spectra to examine the wavelength-dependence of photosynthetic quantum yield, and found that the spectral quality of the light field had a marked effect on pigmentation and quantum yield. They calculated spectral quantum yield values by dividing the carbon action spectra (α) by the chlorophyll specific absorption coefficient ($\phi(\lambda) = \alpha(\lambda) / a^*_{phi}(\lambda)$).

Figure 10 is an adaptation of the Bidigare et al. quantum yield determinations. Spectral values are binned into 3 categories for convenience in this study, but were binned every 25 nm in Bidigare et al. (1989). The dashed line represents the non-spectral (average) quantum yield for the entire visible spectrum.

Spectral quantum yield values were not found in the literature for the other two groups. For Station 75, alpha values of photosynthesis-light curves reported by Shanley

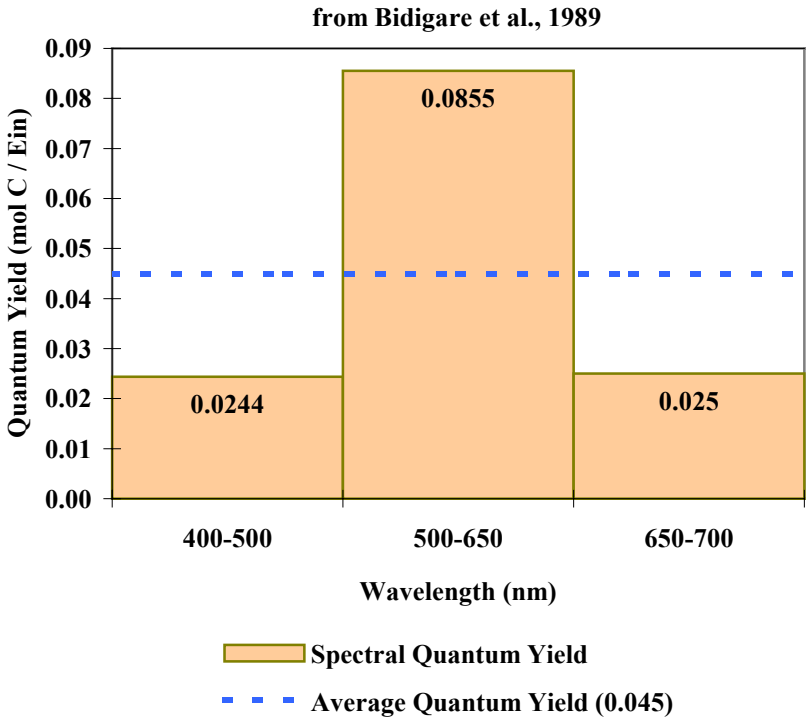

Figure 10. Quantum yield of photosynthesis for *Synechococcus* grown under white light: Spectral and average values. (adapted from (Bidigare et al. 1989)).

(1985) for *K. brevis* cultures were converted to quantum yields. Calculated values of quantum yield of photosynthesis ranged from a minimum of 1.5% to a maximum of 5.3%. These values (1.5% and 5.3%) were used as a minimum and maximum quantum yield of photosynthesis, respectively, for all Station 75 simulations. These minimum and maximum quantum yield values fall within quantum yield ranges reported in the literature for oligotrophic assemblages of cyanophytes and prochlorophytes (Babin et al. 1996) as well as for undetermined assemblages in various natural marine environments (Marra et al. 2000; Schofield et al. 1993; Sorensen and Siegel 2001). Therefore, in order to make direct comparisons for all groups, these values (1.5% and 5.3%) were also used for the Offshore, and Station 72a, bottom comparisons.

3.8 Selection of respiration values

Working with the simplifying assumptions about phytoplankton composition at these stations, representative values for dark respiration were chosen from the literature. For Station 72a, the dark respiration value for a non-iron limited, Bermuda strain of *Synechococcus* (WH7803) grown at 50 μEinsteins m^{-2} s^{-1} (0.12 fmol 0_2 $cell^{-1}$ hr^{-1} = 1.54 x 10^{-4} μg C μg^{-1} chl s^{-1}) was chosen (Henley and Yin 1998). Strain WH7803 belongs to a phycoerythrobilin-dominant group of *Synechococcus*. For Station 75, the dark respiration value for a *Karenia brevis* (formerly, *Ptychodiscus brevis*) culture grown at 90 μEinsteins m^{-2} s^{-1} (4 x 10^{-6} μg C $cell^{-1}$ hr^{-1} = 1.98 x 10^{-4} μg C μg^{-1} chl s^{-1}) was chosen (Shanley 1985).

For the Offshore comparison, a literature search did not reveal specific respiration rates for prochlorophyte species. Therefore the *Synechococcus* respiration rate used for Station 72a was also used for the Offshore comparison. Prochlorophytes are so similar to cyanophytes, that some authors have recommended that they be reclassified as cyanophytes (Urbach et al. 1992). Therefore, a respiration rate for *Synechococcus* was considered a reasonable substitution.

4. RESULTS AND DISCUSSION

4.1 Station 72a

Figure 11 shows a form of Hydrolight model validation using a comparison of measured vs. modeled remote-sensing reflectance. Agreement between measured and modeled R_{rs} infers that the light returned from the water column is similar between measured and modeled values, both qualitatively and quantitatively. This agreement infers that the modeled values for E_o are also qualitatively and quantitatively similar to actual conditions at this station.

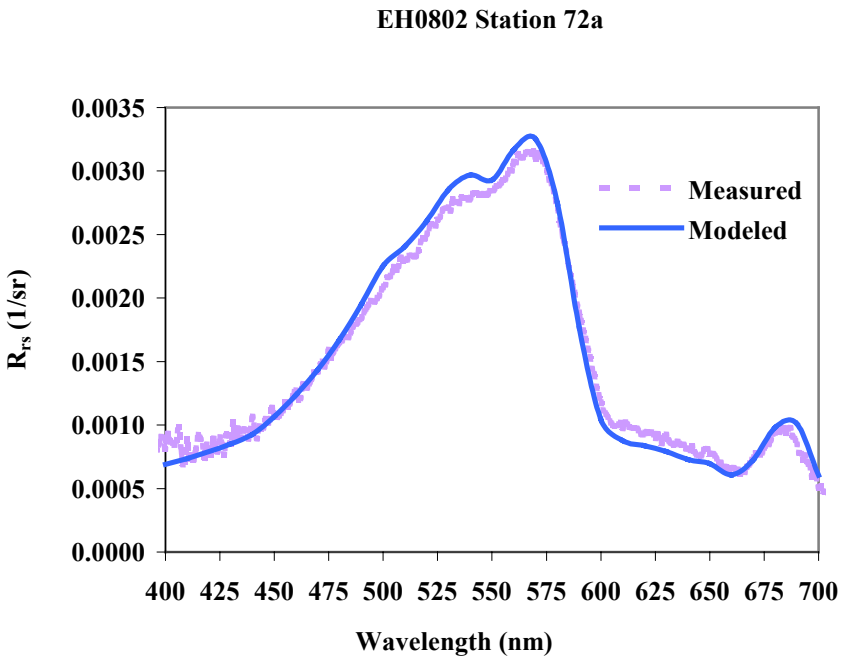

Figure 11. EH0802 Station 72a: Model Validation: Measured vs. modeled remote sensing reflectance.

Figure 12 shows the underwater light field (12a) and absorption by phytoplankton (12b) with depth for Station 72a. These figures reveal that near the surface, most of the absorption by phytoplankton occurred at the blue end of the spectrum, causing the irradiance that is available to, and absorbed by, phytoplankton near the bottom, to shift

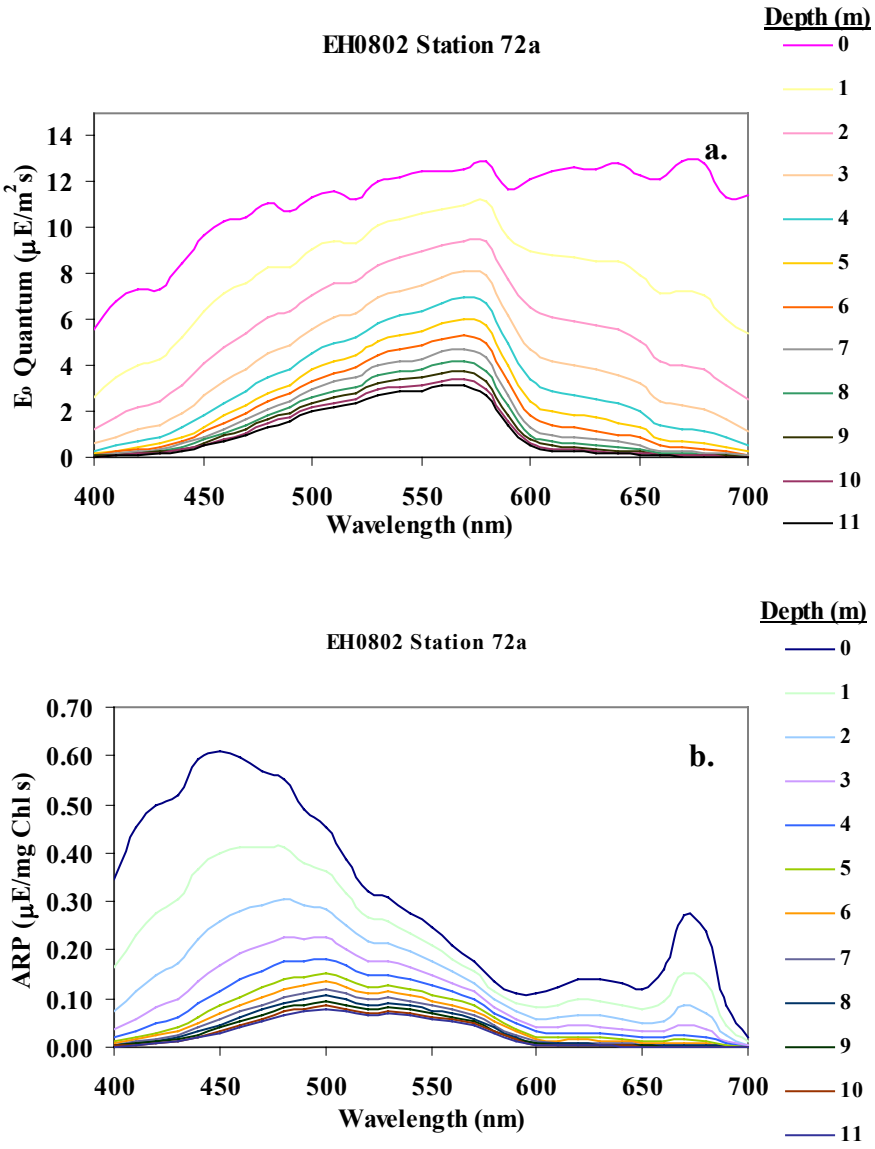

Figure 12. EH0802 Station 72a: a.) Quantum irradiance and b.) Absorbed radiation by phytoplankton from surface to bottom.

toward the blue-green wavelengths. Near the bottom, two absorption peaks emerge at roughly 495 nm and 550 nm. These are regions of peak absorption by the phycobilin pigments, phycourobilin (PU) and phycoerythrobilin (PE), respectively. Therefore, near the bottom, the most efficient regions of light harvesting for this station are the wavelength regions associated with the PE and PU peaks, roughly the same wavelength region of highest quantum yield values reported by Bidigare et al. (1989), as can be seen in Figure 13.

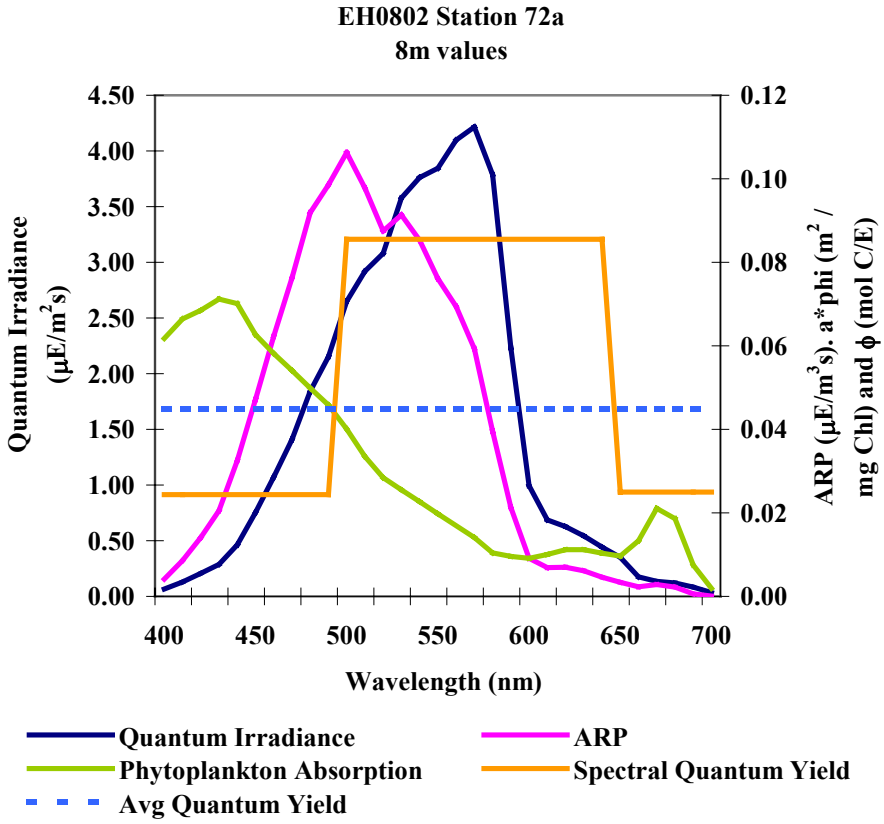

Figure 13. EH0802 Station 72a: Absorbed radiation by phytoplankton and it's components (quantum irradiance and phytoplankton absorption) at 8m depth, compared against spectral and non-spectral quantum yield values for *Synechococcus* (adapted from Bidigare et al., 1989).

Figure 13 shows absorbed radiation by phytoplankton and its components at 8 m depth, compared against spectral and non-spectral quantum yield values (from Bidigare et al., 1989). Note that values for E_o are on a separate axis from the other values. The authors showed that quantum yield can be highly wavelength dependent. The highest quantum yield values for *Synechococcus,* reported by Bidigare et al. (1989), are in the green wavelengths. Near the bottom of the water column, the 500 – 600 nm region of the spectrum appears to be optimal for harvesting and converting photons to photosynthetic product for *Synechococcus* in this simulation. The spectral nature of the quantum yield reveals the importance of the phycobilins, in driving photosynthesis in *Synechococcus* at depth.

Figure 14 and Table 3 are a comparison of calculated net photosynthesis using a spectral (green-rich) quantum yield and a non-spectral (broadband) quantum yield. At the bottom of Station 72, nearly 10% of the surface light remained, and calculated net photosynthesis approaches, but does not go to zero. Therefore the water column at this station was not light-limited. Calculated values of net photosynthesis compare well with measured production values reported by Wawrik et al (2003). The authors measured ^{14}C fixation in incubated water samples from a location in the GOM with a surface (top 10 m) layer dominated by *Synechococcus* species. The photosynthetic carbon fixation maximum for the surface sample was 13.35 mg C mg^{-1} chl hr^{-1}. In this study, calculated values for net production range from 1.7 to 17.2 mg C mg^{-1} chl hr^{-1} over the top 8 m using spectral quantum yield values.

This simulation demonstrates that when the spectral nature of quantum yield is not taken into consideration, net photosynthesis may be underestimated: In the first half

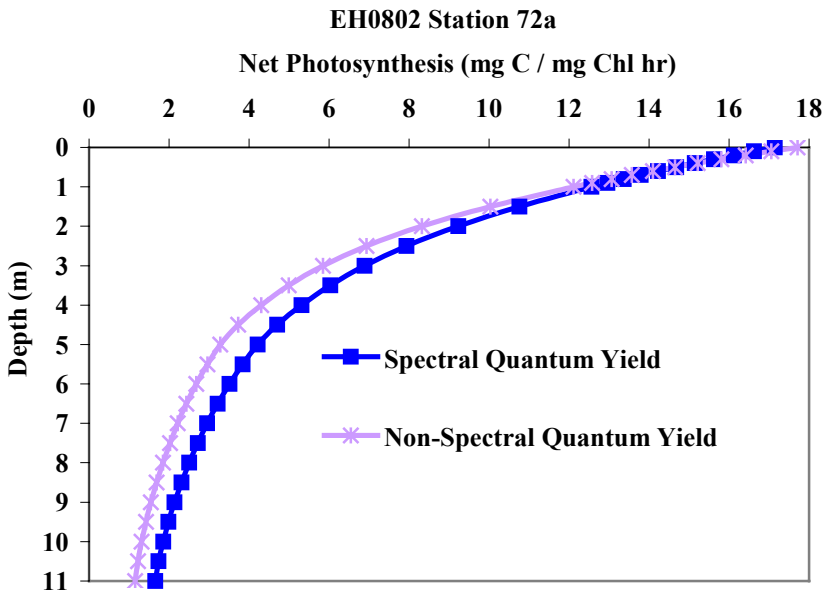

Figure 14. EH0802 Station 72a: Comparison of net photosynthesis calculated using a spectral quantum yield and a non-spectral quantum yield.

meter below the surface, where blue light is the dominant light available, net photosynthesis calculations are slightly higher using the non-spectral quantum yield. However, this includes the effect of photoprotective pigments, as if they are light-harvesting pigments. As the available light shifts toward the blue-green with depth, the spectral quantum yield calculations produce higher net photosynthesis. At the bottom of the first meter, net photosynthesis calculated with a spectral quantum yield is only 4% greater than photosynthesis calculated with a non-spectral quantum yield. At a depth of 11 meters, the difference rises to over 30%.

Table 3 shows that the presence of absorption by phycoerythrobilin (PE), in the Station 72a water column yielded only minor differences in the calculated rate of net photosynthesis throughout the water column than a phytoplankton population might without this absorption feature. The “w/PE” net photosynthesis calculations are about 6%

		Net Photosynthesis (mg C mg^{-1} chl hr^{-1})			
Depth	% Light	"PE"		"No PE"	
(meters)	Level	Spectral ϕ	Non-Spectral ϕ	Spectral ϕ	Non-Spectral ϕ
0	100%	17.15	17.71	16.08	17.15
1	71%	12.56	12.11	11.70	11.66
2	51%	9.23	8.32	8.54	7.96
3	38%	6.89	5.85	6.35	5.56
4	29%	5.31	4.30	4.87	4.07
5	23%	4.21	3.28	3.85	3.09
6	19%	3.51	2.68	3.20	2.52
7	16%	2.95	2.22	2.69	2.08
8	14%	2.50	1.85	2.28	1.73
9	12%	2.14	1.55	1.95	1.45
10	11%	1.85	1.31	1.68	1.23
11	10%	1.66	1.16	1.50	1.07

Table 3. EH0802 Station 72a: Comparative values of net photosynthesis for “w/PE” and “No PE” Hydrolight runs, using spectral vs. non-spectral quantum yield. Percent of surface light remaining with depth is also shown.

higher at the surface increasing to about 10% at the bottom, using a spectral quantum yield. In this relatively well-mixed, non light-limited water column, the additional light harvesting provided by PE may not provide a major advantage to a group of phytoplankton. However, as will be seen in the results of the deep comparisons, in a light-limited water column, the presence of PE may allow a phytoplankton group to exhibit positive net production to a greater depth than a group without PE.

4.2 Station 75

Figure 15 shows the modeled quantum irradiance and Figure 16 shows the absorbed radiation by phytoplankton at Station 75 from just below the surface to the

bottom. In the first meter below the surface, the amount of available blue light drops dramatically. At a depth of 5 m, there is virtually no blue light remaining. Red light is also rapidly diminished in the water column, especially at the chl *a* absorption peak, around 675 nm. As depth increases, a relatively narrow window of light centered around 570 nm and a smaller window around 650 nm remain.

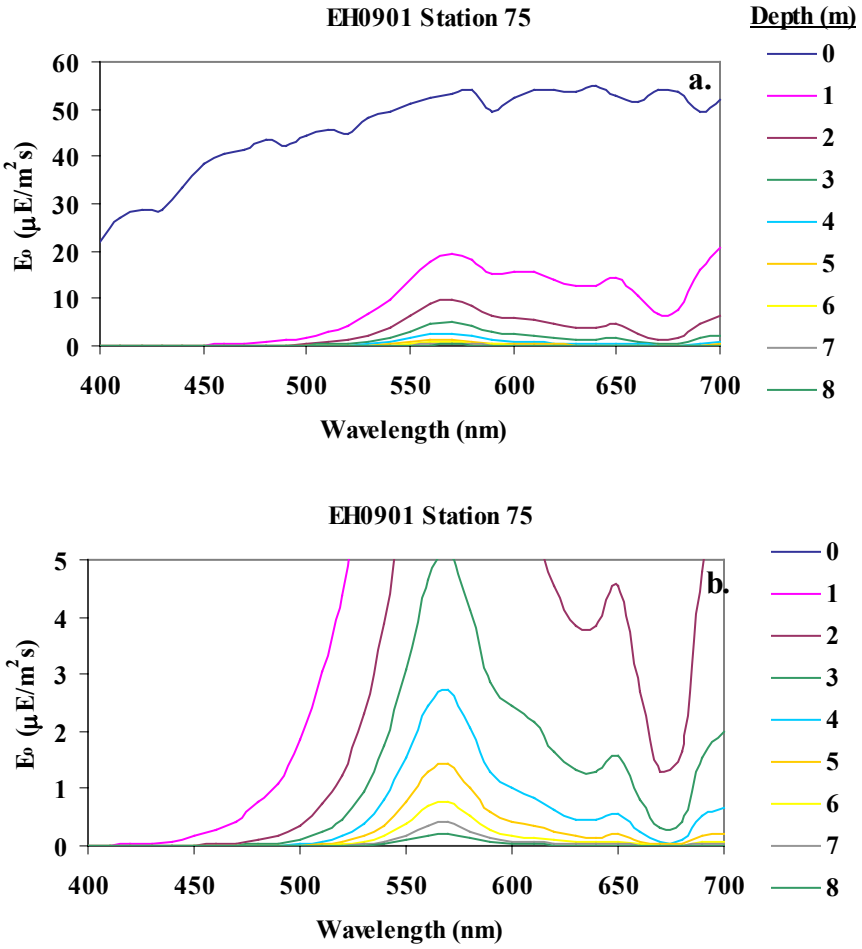

Figure 15. EH0901 Station 75: Quantum irradiance a.) from surface to bottom and b.) close-up of the bottom of the water column.

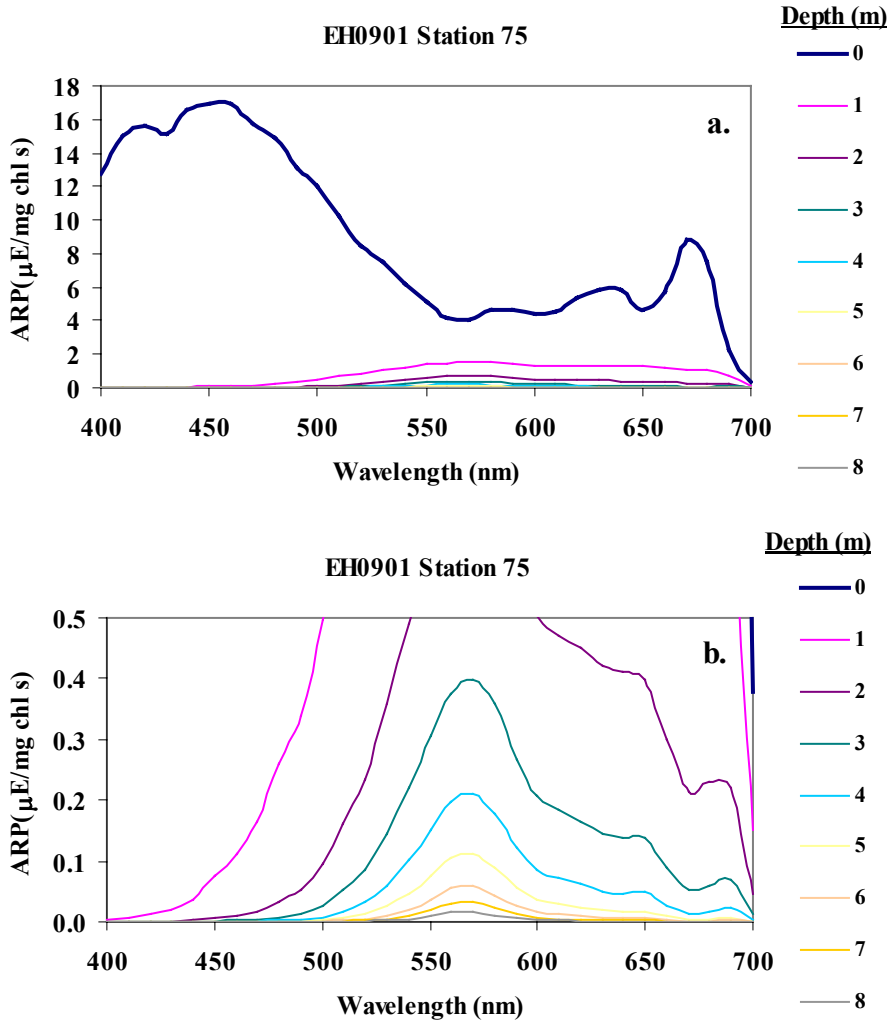

Figure 16. EH0901 Station 75: Absorbed radiation by phytoplankton a.) from surface to bottom and b.) close-up of the bottom of the water column.

K. brevis contains light-harvesting pigments, including chlorophylls *a, c*$_1$*, c*$_2$*, c*$_3$ and fucoxanthins, as well as, photoprotective carotenoids, including diadinoxanthin and diatoxanthin, that collectively absorb throughout the blue wavelengths (Jeffrey et al. 1997; Millie et al. 1997). Table 4 shows the major and minor absorption peaks for these pigments. All have their major absorption peaks in the blue region of the spectrum. At a depth of 5 m, there is no blue light remaining for these pigments to absorb. Therefore, at

this depth, K.brevis would have to rely on the minor absorption peaks in the yellow and red wavelengths of the chlorophylls to harvest light for photosynthesis.

K. brevis Major Pigments	Major (Minor) Abs Peaks	Function
Fucoxanthins	**445, (470)**	**LH**
Chl a	**430, (662)**	**LH**
Diadinoxanthin	**(425), 448, 478**	**PP**
Diatoxanthin	**(427), 454, 482**	**PP**
Chl c_1	**446, (578, 628)**	**LH**
Chl c_2	**450, (581, 630)**	**LH**
Chl c_3	**452, (585,626)**	**LH**

Table 4. Major pigments in *Karenia brevis* (Jeffrey 1980; Jeffrey et al. 1997; Morel 1997). Absorption peaks are in acetone solvent. LH: Light-Harvesting, PP: Photoprotective.

Figure 17 and Table 5 compare simulated net photosynthesis through the water column, calculated with practical maximum- (5.3%) and minimum- (1.5%) quantum yields. At both quantum yield values, phytoplankton in this simulation would reach a compensation point (i.e. exhibit zero net photosynthesis) well above the bottom. Using ϕ_{min}, this compensation point would occur between 4 – 4.5 m depth, roughly the same depth as the 1% light level. Using ϕ_{max}, the compensation point would occur between 6 - 6.5 m depth. Shanley (1985) reported a compensation intensity for *K. brevis* of 5.6 μEin m^{-2} s^{-1}, which falls between 5-6 m depth at this station (see Table 4).

Calculated values of net photosynthesis using ϕ_{min} compare well with measured production values reported by Shanley (1985). The author reported maximum photosynthesis (P_{max}) values ranging from 0.29 – 5.37 mg C mg^{-1} chl hr^{-1} for cultures of

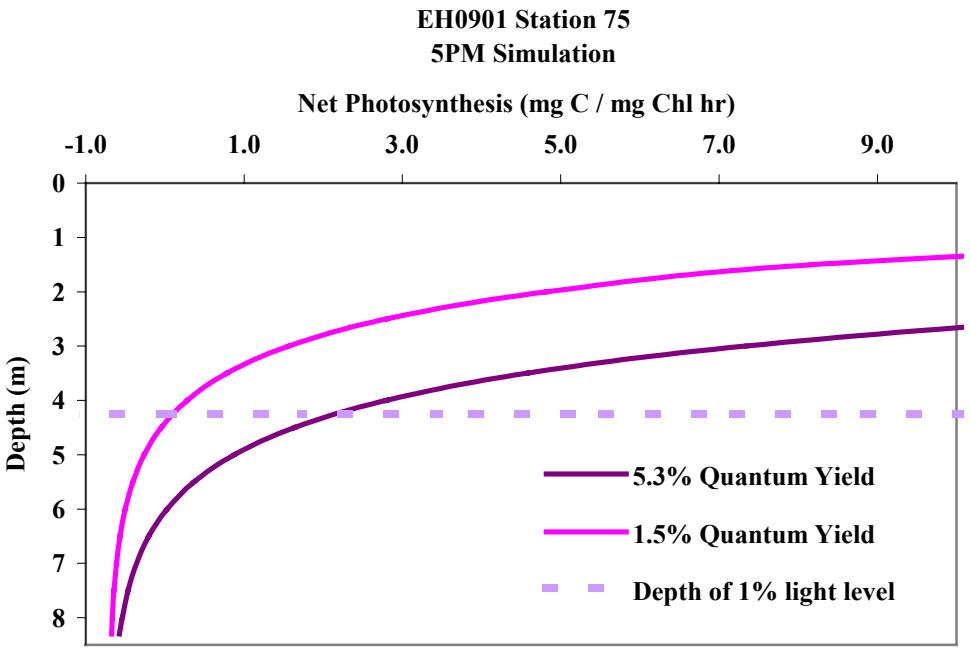

Figure 17. EH0901 Station 75: Net photosynthesis with depth calculated using a maximum and minimum quantum yield. Depth is shown in 1 m increments and the 1% light level is indicated by the dashed line.

K. brevis grown at light levels ranging from 24 – 160 μEin m^{-2} s^{-1}. In this study, calculated values for net production for irradiances from 26 – 150 μEin m^{-2} s^{-1} range from 0.78 – 8.17 mg C mg^{-1} chl hr^{-1} using ϕ_{min} and 4.57 – 30.7 mg C mg^{-1} chl hr^{-1} using ϕ_{max}, for the 5 PM simulation. Values are similar for the noon simulation. Bendis et al. (2002) reported a range of P_{max} values of 0.29 – 5.9 mg C mg^{-1} chl hr^{-1} for *K. brevis* cultures sampled from the GOM with cell counts > 10^5 cells L^{-1}. Calculated values for net production using ϕ_{min} are closer to those measured by Shanley and Bendis et al. *K. brevis* is a slow-growing, low-light-adapted dinoflagellate, with doubling times of less than 1 per day (Shanley 1985; Steidinger et al. 1998). Therefore at higher light levels, a lower

5pm Simulation					Noon Simulation				
Depth (m)	E_o ($\mu E\ m^{-2}\ s^{-1}$)	% Light Level	Net Photosynthesis (mg C mg-1 chl hr-1) (5.3% ϕ)	(1.5% ϕ)	Depth (m)	E_o ($\mu E\ m^{-2}\ s^{-1}$)	% Light Level	Net Photosynthesis (mg C mg-1 chl hr-1) (5.3% ϕ)	(1.5% ϕ)
0	1421.59	100.0%	629.32	177.60	0	2033.26	100.0%	930.56	262.85
1	259.49	18.3%	56.20	15.40	1	485.98	23.9%	110.35	30.72
1.5	149.64	10.5%	30.67	8.17	1.5	351.17	17.3%	75.02	20.72
2	93.53	6.6%	18.81	4.81	2	236.18	11.6%	49.70	13.56
2.5	59.91	4.2%	11.73	2.81	2.5	158.34	7.8%	32.79	8.77
3	38.98	2.7%	7.34	1.57	3	106.44	5.2%	21.64	5.62
3.5	25.68	1.8%	4.57	0.78	3.5	71.87	3.5%	14.29	3.53
4	17.10	1.2%	2.79	0.28	4	48.77	2.4%	9.41	2.15
4.5	11.49	0.8%	1.64	-0.05	4.5	33.28	1.6%	6.16	1.23
5	7.79	0.5%	0.87	-0.26	5	22.82	1.1%	3.98	0.62
5	5.32	0.4%	0.37	-0.41	5.5	15.73	0.8%	2.51	0.20
6	3.65	0.3%	0.03	-0.50	6	10.89	0.5%	1.51	-0.08
6.5	2.53	0.2%	-0.20	-0.57	6.5	7.57	0.4%	0.83	-0.28
7	1.75	0.1%	-0.36	-0.61	7	5.29	0.3%	0.36	-0.41
7.5	1.22	0.1%	-0.47	-0.64	7.5	3.71	0.2%	0.04	-0.50
8	0.86	0.1%	-0.54	-0.66	8	2.60	0.1%	-0.19	-0.56
8.3	0.68	0.0%	-0.58	-0.67	8.3	2.08	0.1%	-0.29	-0.59

Table 5. EH0901 Station 75: Comparative values of net photosynthesis for "5 PM" and "Noon" Hydrolight runs, using a maximum and minimum quantum yield. Quantum irradiance with depth and percent light remaining are also shown. Negative net photosynthesis values are highlighted in gray; the approximate depths of the 1% light level is highlighted in yellow; and the approximate depths of the compensation point reported by Shanley (1985) are highlighted in blue.

quantum yield would be expected. Only at very low light levels (e.g. the bottom few meters) would one expect *K. brevis* to exhibit a relatively high quantum yield.

Figure 18 compares the Hydrolight-simulated absorbed radiation by phytoplankton at the bottom 4 m of Station 75 at 5 PM and noon. As with Figure 16b, in

the bottom half of the water column, light harvesting is mainly occurring in the green region of the spectrum, because there is no blue light available at these depths. At noon, the spectral quality of the light at depth remains the same, but the quantity is greater; therefore the phytoplankton are absorbing larger quantities of radiation at the same wavelengths than at 5 PM. In this simulation, phytoplankton are absorbing 2.5 – 3.5 times more light at noon than at 5 PM in the bottom half of the water column. This difference in light absorption translates into a 1.5 m difference in the depth of the calculated compensation point between the 5 PM and noon simulations (Table 4).

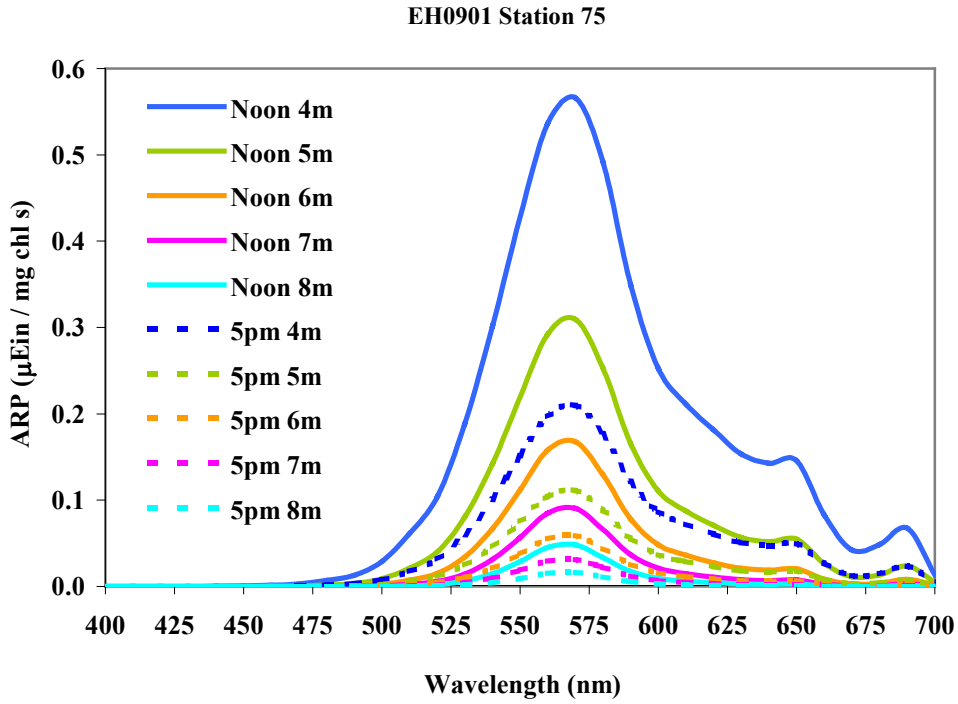

Figure 18. EH0901 Station 75: Comparison of absorbed radiation by phytoplankton at Station 75 for the "5 PM" and "Noon" Hydrolight runs at the bottom 4 meters of Station 75.

As expected, Figure 18 and Table 3 reveal higher net photosynthesis with depth at noon than at 5 PM. At noon, the depth where negative net photosynthesis occurs is 1.5 m deeper than at 5 PM, indicating that the phytoplankton at this station are viable at greater depth at noon. However, neither simulation yields positive net photosynthesis all the way to the bottom, so even at noon, Station 75 remains a light-limited environment near the bottom.

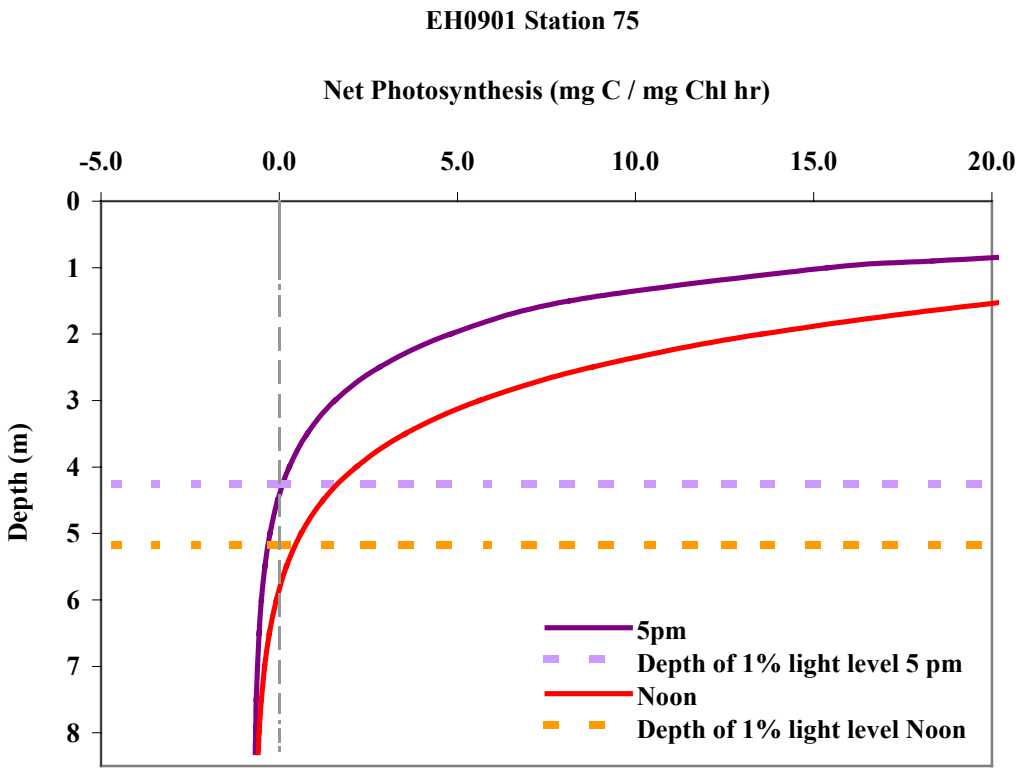

Figure 19. EH0901 Station 75: Comparison of net photosynthesis with depth for the "5 PM" and "Noon" Hydrolight runs (calculated using the minimum quantum yield). The 1% light levels are indicated by the dashed lines.

4.3 Deep comparisons

Figure 20 compares the absorbed radiation by phytoplankton in the bottom meter of the water column for the deep comparison simulations. Figure 20a shows ARP for the four representative phytoplankton groups over a Station 72a "No PE" water column, while Figure 20b is over a Station 75 water column. Both are simulations for 5 PM.

For the Station 72a comparison, the "Offshore" phytoplankton absorb more light per unit chlorophyll than the other groups in the blue-green region of the spectrum, but at about 525 nm, absorption drops below that of the other three groups, then to virtually zero above 600 nm.

Prochlorophytes contain light-harvesting (including divinyl chl *a*, and divinyl chl *b*) and photoprotective (including zeaxanthin) pigments (Table 6) that absorb strongly in the blue region of the spectrum, contributing to their ability to harvest blue wavelengths (Jeffrey et al. 1997; Millie et al. 1997). Their small cell sizes (<1 μm diameter) contribute to a very low "package effect" (Bricaud et al. 1983) and high absorption efficiencies. Based upon these differences in pigmentation and the results shown in Fig. 20a, one would not expect the prochlorophytes from this station to compete effectively in a. CDOM-rich environment, such as Station 75, that would remove light from the shorter end of the spectrum, while the phycobiliprotein-containing phytoplankton would be better-suited to harvest the green-rich light at the bottom.

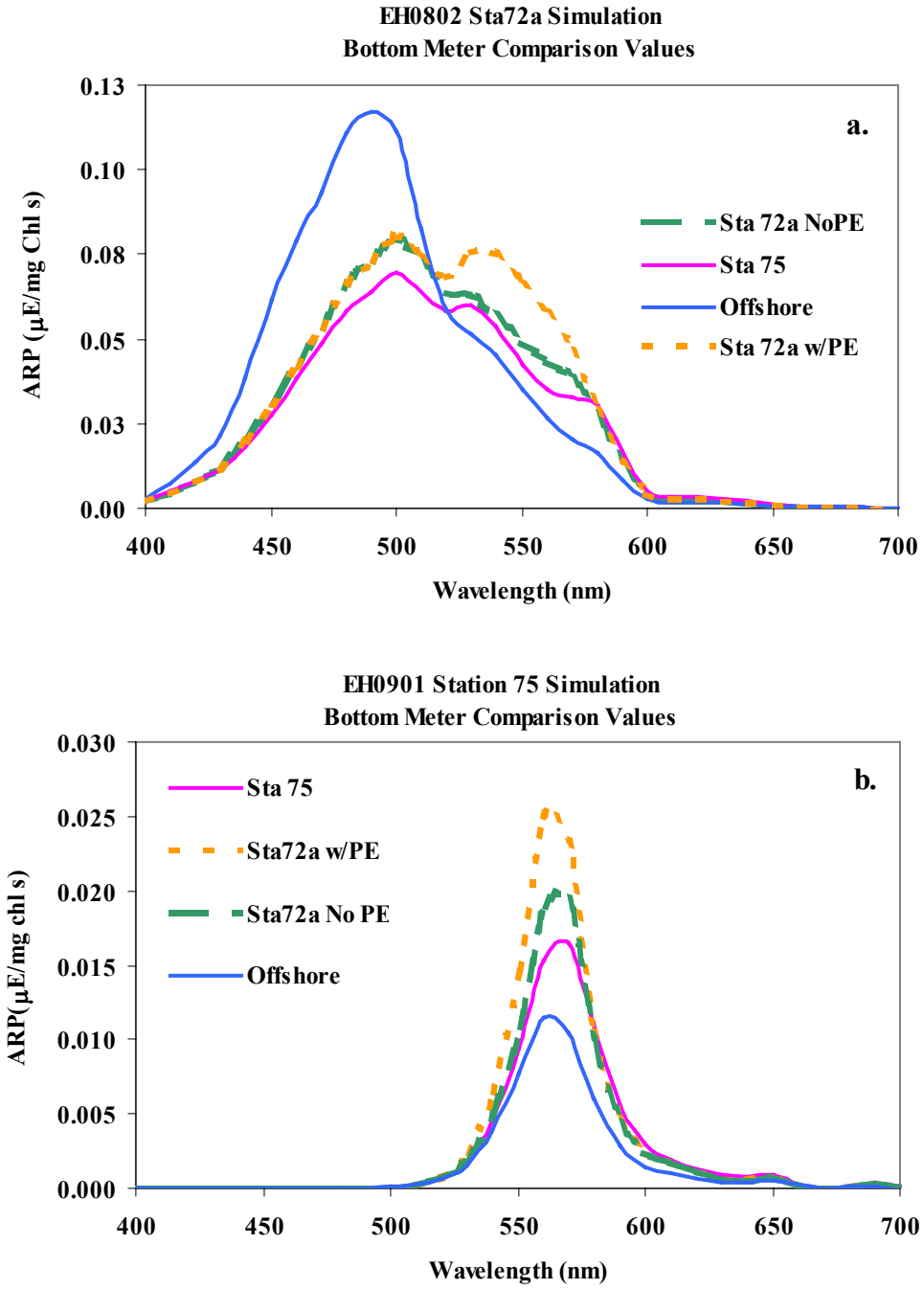

Figure 20. Comparison of absorbed radiation by phytoplankton at the bottom meter for various phytoplankton groups a.) below an upper layer with phytoplankton absorption with no phycoerythrin peak ("No PE") b.) below an upper layer with phytoplankton absorption from the Station 75 *K. brevis* bloom. The same maximum and minimum quantum yield values are used for all simulations.

Prochlorophytes Major Pigments	Major (Minor) Abs Peaks	Function
Divinyl Chl *a*	**442, 666**	**LH**
Divinyl Chl *b*	**460,644**	**LH**
Zeaxanthin	**(428), 454, 481**	**LH/PP**

Table 6. Major pigments in prochlorophytes (Jeffrey 1980; Jeffrey et al. 1997; Morel 1997). Absorption peaks are in acetone solvent. LH: Light-Harvesting, PP: Photoprotective.

At Station 75, all the blue light is rapidly absorbed in the first few meters (refer to Figure 14), therefore in the bottom meter, only a narrow band of light remains, roughly between 525 - 600 nm, that is available for absorption by phytoplankton. Under these conditions, the PE-containing phytoplankton (the "w/PE" ARP curve) apparently absorb the most light, while the Offshore, prochlorophyte-dominated group absorbs the least.

Table 7a compares net photosynthesis in the bottom meter for various phytoplankton groups below an upper layer with phytoplankton absorption with no phycoerythrin peak from Station 72a ("No PE"). All of the modeled groups exhibit positive net photosynthesis at the maximum quantum yield value. The Offshore group, however, exhibits a higher rate of net photosynthesis than the other groups. In this simulation, the Offshore group would out-compete the others because there is more blue light near the bottom for this simulation. In this case, the prochlorophytes in this group have an advantage at this station in that they contain light-harvesting and photoprotective pigments that absorb strongly in the blue region of the spectrum, allowing them to harvest the available blue light more effectively than the other groups. The PE-containing

group does not absorb the available blue wavelengths as well as the Offshore group in this simulation, but there is also enough green light remaining at the bottom of this station for it to exhibit the second-highest calculated net production. The *K. brevis* group exhibited the lowest absorption and lowest production in this simulation.

Calculated values of net photosynthesis for *Synechococcus* at Station 72a and *K. brevis* at Station 75 compared well with measured production values as discussed previously. Calculated net photosynthesis values for prochlorophytes in the Station 72a simulation also compare well with measured production values in the literature for a GOM prochlorophyte, *Prochlorococcus*. In Wawrik et al. (2003), the authors measured ^{14}C fixation in incubated water samples from a location in the GOM with a subsuface (40 m depth) layer dominated by *Prochlorococcus*. The photosynthetic carbon fixation maximum for this sample was 4.2 mg C mg^{-1} chl hr^{-1}. In this study, calculated values for net production of the Offshore prochlorophyte group in the bottom meter range from 0.1 to 2.0 mg C mg^{-1} chl hr^{-1} at 5 PM and likely three times as much at noon.

Table 7b compares net photosynthesis in the bottom meter for various phytoplankton groups below an upper layer with phytoplankton absorption from the Station 75 *K. brevis* bloom. In this simulation, none of the groups exhibits net positive photosynthesis near the bottom at 5 PM, but if these results are extrapolated toward the surface, Station 72a "w/PE" group would have the deepest compensation depth, excelling over the other groups in light harvesting ability in this green-rich light environment. PE and the other biliproteins absorb most strongly in the green region of the spectrum, explaining the success of this biliprotein-containing group at the bottom of this CDOM-rich station, where only a narrow window of green light reaches the bottom. In this

simulaton, the Offshore group exhibits the lowest absorption of all the groups due to its lack of green-light absorbing pigments. *K. brevis* also lacks green-light absorbing pigments, but the secondary chl *c* absorption peaks in the yellow give it an absorption advantage over the Offshore prochlorophytes that have no major pigments with absorption peaks in the green or yellow region of the spectrum. Nevertheless, it is the *K. brevis* group that exhibits the lowest net production in this simulation, due to its lack of green-light absorbing pigments combined with its higher respiration rate.

a.

Sta 72a No PE Curve Simulation
Net Photosynthesis (mg C mg^{-1} chl hr^{-1})

Depth (m)	Sta72a No PE (*Synechococcus*) (5.3% ϕ)	Sta72a No PE (*Synechococcus*) (1.5% ϕ)	Sta72a w/ PE (*Synechococcus*) (5.3% ϕ)	Sta72a w/ PE (*Synechococcus*) (1.5% ϕ)	Offshore (Prochlorophytes) (5.3% ϕ)	Offshore (Prochlorophytes) (1.5% ϕ)	Sta 75 (*K.brevis*) (5.3% ϕ)	Sta 75 (*K.brevis*) (1.5% ϕ)
10	1.54	0.04	1.73	0.09	1.99	0.17	1.20	-0.17
10.5	1.44	0.01	1.62	0.06	1.86	0.13	1.11	-0.20
11	1.37	-0.01	1.54	0.04	1.77	0.10	1.04	-0.22

b.

Sta 75 5PM Simulation
Net Photosynthesis (mg C mg^{-1} chl hr^{-1})

Depth (m)	Sta72a No PE (*Synechococcus*) (5.3% ϕ)	Sta72a No PE (*Synechococcus*) (1.5% ϕ)	Sta72a w/ PE (*Synechococcus*) (5.3% ϕ)	Sta72a w/ PE (*Synechococcus*) (1.5% ϕ)	Offshore (Prochlorophytes) (5.3% ϕ)	Offshore (Prochlorophytes) (1.5% ϕ)	Sta 75 (*K.brevis*) (5.3% ϕ)	Sta 75 (*K.brevis*) (1.5% ϕ)
10	-0.29	-0.48	-0.24	-0.46	-0.39	-0.51	-0.47	-0.64
10.5	-0.37	-0.50	-0.33	-0.49	-0.44	-0.52	-0.54	-0.66
11	-0.41	-0.51	-0.38	-0.50	-0.46	-0.53	-0.58	-0.67

Table 7. Comparison simulations of net photosynthesis at the bottom meter for various phytoplankton groups a.) above an upper layer with phytoplankton absorption with no phycoerythrin peak ("No PE") b.) above an upper layer with phytoplankton absorption from the Station 75 *K. brevis* bloom. The phytoplankton groups exhibited the highest and lowest net photosynthesis rates are highlighted in yellow and gray, respectively. Negative net photosynthesis values are also highlighted in gray.

In both near-bottom comparison simulations, *K. brevis* was out-competed by other phytoplankton groups. This is partly due to its higher respiration rate and partly due to its lack of major green-light absorbing pigments. Then why is this "nuisance species" so successful on the WFS? The ability to take advantage of available wavelengths at depth is apparently not the answer. As mentioned in the introduction, nutrient and grazing dyanamics, were not considered in this study. Adaptive strategies such as efficient uptake and utilization of organic and inorganic nutrients, and production of brevetoxins that discourage grazing (Steidinger et al. 1998), may be more important than pigment/light field compatibility to the success of *K. brevis*, especially considering that *K.brevis* is motile (Heil 1986), allowing it to swim upward in the water column toward more favorable light conditions.

5. CONCLUSIONS

This study successfully demonstrates a technique for extracting information about the water column and the optical niche it represents, even in the absence of underwater irradiance measurements. It may prove to be a useful technique for investigations, such as the ECOHAB surveys, in which time constraints don't allow thorough evaluation of underwater optical properties at each station. This study simulated $E_o(\lambda, z)$ and $ARP(\lambda, z)$ for natural phytoplankton populations throughout the water column, making it possible to examine how phytoplankton utilize the light field with depth, and how the optical properties of the water column are influenced by phytoplankton.

Results of these simulations suggest that, in a shallow or well-mixed water column, possessing pigments that are well-matched to the near-bottom light field does not represent an important competitive advantage to a group of phytoplankton. However, in a water column that is not well-mixed, or where light may be limited, it will be more important for a group of phytoplankton to have pigments that are well-matched to the light field. For example, in the deep comparisons of this study, the presence of green-light absorbing biliproteins in cyanophytes and yellow-light absorbing chlorophyll *c* in *K. brevis* were critical to their ability to absorb enough photons to meet their metabolic requirements, near the bottom of a light-limited water column, in which all blue light was extinguished.

The spectral quality of the light field, as well as, the wavelength-dependence of chlorophyll specific absorption and quantum yield, are important considerations in accurately modeling ocean primary production. ARP and production at depth may be underestimated if the spectral nature of these variables is not considered. The degree of error introduced in incubation experiments and models that do not take this into consideration will depend upon the pigment suite and the level of photo-adaptation to the light environment of the phytoplankton studied. It will also depend on the spectral character of the light field. The results of this study suggest the need to accurately mimic both the intensity and the spectral quality of the underwater light field in incubation experiments, and the need for more investigations of the spectral character of quantum yield and chlorophyll specific absorption of phytoplankton.

REFERENCES

BABIN, M., A. MOREL, H. CLAUSTRE, A. BRICAUD, Z. KOLBER, and P. G. FALKOWSKI. 1996. Nitrogen- and irradiance-dependent variations of the maximum quantum yield of carbon fixation in eutrophic, mesotrophic and oligotrophic marine systems. Deep Sea Res. **43:** 1241-1272.

BENDIS, B., R. PIGG, D. MILLIE, and K. STEIDINGER. 2002. Primary productivity of Florida red tides. *In* K. A. Steidinger, J. H. Landsberg, C. R. Tomas and G. A. Vargo [eds.]. Florida Fish and Wildlife Conservation Commission and Intergovernmental Oceanographic Commission of UNESCO.

BIDIGARE, R. R., M. E. ONDRUSEK, and J. M. BROOKS. 1993. Influence of the Orinoco River outflow on distributions of algal pigments in the Caribbean Sea. J. Geophys. Res. **98:** 2259-2269.

BIDIGARE, R. R., O. SCHOFIELD, and B. B. PREZELIN. 1989. Influence of zeaxanthin on quantum yield of photosynthesis of Synechococcus clone WH7803 (DC2). Marine Ecology Progress Series **56:** 177-188.

BIDIGARE, R. R., R. C. SMITH, K. S. BAKER, and J.MARRA. 1987. Oceanic primary production estimates from measurements of spectral irradiance and pigment concentrations. Global Biogeochemical Cycles **1:** 171-186.

BRICAUD, A., A. MOREL, and L. PRIEUR. 1983. Optical efficiency factors of some phytoplankters. Limnology and Oceanography **28:** 816-832.

CANNIZZARO, J. P., K. L. CARDER, F. R. CHEN, J. J. WALSH, Z. P. LEE, and C. HEIL. 2002. A novel optical classification technique for detection of red tides in the Gulf of Mexico: application to the 2001-2002 bloom event, p. 4. *In* J. H. L. K.A. Steidinger, C.R. Tomas, G.A. Vargo [ed.], Florida Fish and Wildlife Conservation Commission and Intergovernmental Oceanographic Commission of UNESCO. Intergovernmental Oceanographic Commission of UNESCO.

CARDER, K. L., F.R. CHEN, Z.P. LEE, S.K. HAWES, D. KAMYKOWSKI. 1999. Semianalytic Moderate-Resolution Imaging Spectrometer algorithms for chlorophyll a and absorption with bio-optical domains based on nitrate-depletion temperatures. Journ. Geophys. Res. **104:** 5403-5421.

FARMER, C. T., C. A. MOORE, R. G. ZIKA, and R. J. SIKORSKI. 1993. Effects of low and high Orinoco River Flow on the underwater light field of the eastern Caribbean Basin. Journ. Geophys. Res. **98:** 2279-2288.

HEIL, C. A. 1986. Vertical migration of Ptycodiscus brevis (Davis) Steidinger, p. 118. University of South Florida.

HENLEY, W. J., and Y. YIN. 1998. Growth and photosynthesis of marine Synechococcus (Cyanophyceae) under iron stress. J. Phycol **34:** 94-103.

HOEPFFNER, N., and S. SATHYENDRANATH. 1991. Effect of pigment composition on absorption properties of phytoplankton. Marine Ecology Progress Series **73:** 11-23.

HOLM-HANSEN, O. 1978. Chlorophyll a determination: improvements in methodology. OIKOS **30:** 438-447.

JEFFREY, S. W. 1980. Algal pigment systems, p. 33-58. *In* P. G. Falkowski [ed.], Primary Productivity in the Sea. Plenum Press.

JEFFREY, S. W., R. F. C. MANTOURA, and S. W. WRIGHT. 1997. Phytoplankton pigments in oceanography. United Nations educational, scientific and cultural organization.

KIEFER, D. A., and J. B. SOOHOO. 1982. Spectral absorption by marine particles of coastal waters of Baja California. Limnology and Oceanography **27:** 492-499.

KIRK, J. T. O. 1994. Light & Photosynthesis in Aquatic Ecosystems, 2nd ed.**:** 509.

KIRKPATRICK, G. J., D. F. MILLIE, M. A. MOLINE, and O. SCHOFIELD. 2000. Optical discrimination of a phytoplankton species in natural mixed populations. Limnology and Oceanography **45:** 467-471.

LAWS, E. A., G. R. DITULLIO, K. L. CARDER, P. R. BETZER, and S. HAWES. 1990. Primary production in the deep blue sea. Deep-Sea Research **37A:** 715-730.

LEE, Z., K. L. CARDER, C. D. MOBLEY, R. G. STEWARD, and J. S. PATCH. 1999a. Hyperspectral remote sensing for shallow waters. 2. Deriving bottom depths and water properties by optimization. Applied Optics **38:** 3831-3843.

LEE, Z. P., K. L. CARDER, C. D. MOBLEY, R. G. STEWARD, and J. S. PATCH. 1999b. Hyperspectral remote sensing for shallow waters: 2. Deriving bottom depths and water properties by optimization. Applied Optics **38:** 3831-3843.

LEE, Z. P., K. L. CARDER, R. G. STEWARD, T. G. PEACOCK, C. O. DAVIS, and J. L. MUELLER. 1996. Remote-sensing reflectance and inherent optical properties of oceanic waters derived from above-water measurements. Proc. SPIE int. soc. opt. eng. **2963:** 160-166.

MARRA, J., C. C. TREES, R. R. BIDIGARE, and R. T. BARBER. 2000. Pigment absorption and quantum yields in the Arabian Sea. Deep Sea Res. II **47:** 1279-1299.

MILLIE, D. F., O. M. SCHOFIELD, G. J. KIRKPATRICK, G. JOHNSEN, P. A. TESTER, and B. T. VINYARD. 1997. Detection of harmful algal blooms using photopigments and absorption signatures: A case study of the Florida red tide dinoflagellate, Gymnodinium breve. Limnology and Oceanography**.42:** 1240-1251.

MOBLEY, C. D. 1994. Light and Water: Radiative Transfer in Natural Waters. Academic Press.

MOBLEY, C. D. and others 1993. Comparison of numerical models for computing underwater light fields. Applied Optics **32:** 7484-7504.

MOREL, A. 1974. Optical properties of pure water and pure sea water, p. 1-24. *In* N. G. Jerlov and e. s. Nielsen [eds.], Optical aspects of oceanography. academic.

MOREL, A. 1997. Consequences of a Synechococcus bloom upon the optical properties of oceanic (case 1) waters. Limnology and Oceanography **42:** 1746-1754.

POPE, R. M., and E. S. FRY. 1997. Absorption spectrum (380-700 nm) of pure water. II. Integrating cavity measurements. Applied Optics **36:** 8710-8723.

SCHOFIELD, O., B. B. PREZELIN, R. R. BIDIGARE, and R. C. SMITH. 1993. *In situ* photosynthetic quantum yield. Correspondence to hydrographic and optical variability within the Southern California Bight. Mar. Ecol. Prog. Ser. **93:** 25-37.

SHANLEY, E. 1985. Photoadaptation in the red tide dinoflagellate Ptychodiscus brevis. University of South Florida.

SMITH, R. C., and K. BAKER. 1981. Optical properties of the clearest natural waters. Applied Optics **20:** 177-184.

SORENSEN, J. C., and D. A. SIEGEL. 2001. Variability of the effective quantum yield for carbon assimilation in the Sargasso Sea. Deep Sea Res. II **48:** 2005-2035.

STEIDINGER, K. A., G. A. VARGO, P. A. TESTER, and C. R. TOMAS. 1998. Bloom dynamics and physiology of *Gymnodinium breve*, with emphasis on the Gulf of Mexico, p. 135-153. *In* E. M. Anderson, A. D. Cembella and G. M. Hallengraff [eds.], Physiological Ecology of Harmful Algal Blooms. Springer-Verlag.

URBACH, E., D. L. ROBERTSON, and S. W. CHISHOLM. 1992. Multiple evolutionary origins of prochlorophytes within the cyanobacterial radiation. Nature **355:** 267-269.

WALSH, J. J., K. L. CARDER, and F. E. MULLER-KARGER. 1992. Meridional fluxes of dissolved organic matter in the North Atlantic Ocean. Journal of Geophysical Research **97:** 15625-15637.

WAWRIK, B., J. H. PAUL, D. A. BRONK, D. JOHN, and M. GRAY. 2004. High rates of ammonium recycling drive phytoplankton productivity in the offshore Mississippi River plume. Aquatic Microbial Ecology **in press**.

WAWRIK, B. and others 2003. Vertical structure of the phytoplankton community associated with a coastal plume in the Gulf of Mexico. Marine Ecology Progress Series **251:** 87-101.

YENTSCH, C. S. 1962. Measurement of visible light absorption by particulate matter in the ocean. Limnology and Oceanography **7:** 207-217.

APPENDICES

Appendix A: Hydrolight 4.1 Input Parameters

Hydrolight 4.1 Parameter	**EH0802 Station 72a**	**EH0901 Station 75**
Component 1: Pure Water	Pope and Fry, 1997	Pope and Fry, 1997
Component 2: Chlorophyll		
Chlorophyll Concentration (depth profile)	Derived from measured chl concentrations at the surface and 8 m, and chlorophyll fluorescence profile.	Derived from measured chl concentrations and chlorophyll fluorescence profile. An average value is used for Layer 1 (140.1 mg/m^3) and Layer 2 (2.8 mg/m^3).
Chlorophyll specific absorption coefficient ($a^*_{phi}(\lambda)$)	Derived from measured $a_{phi}(\lambda)$ and derived chl concentrations.	Derived from Lee Optimization model using measured surface a_{phi}.
Scattering coefficient ($b(\lambda)$)	A function of Chl concentration: $b(\lambda) = b_o [Chl]^n (\lambda_o/\lambda)^m$, where b_o= 0.39, λ_o=550nm, n=0.63, m=0.	A function of Chl concentration: $b(\lambda) = b_o [Chl]^n (\lambda_o/\lambda)^m$, where b_o= 0.30, λ_o=550nm, n=0.63, m=0.
Backscattering Efficiency (b_b/b)	0.0072	Layer 1: 0.0078 Layer 2: 0.31
Component 3: CDOM		
Depth profile of absorption coefficient ($a_{CDOM}(420)$).	Regression of $a_{CDOM}(420)$ measurements at the surface and 8m against salinity profile.	Derived from Lee Optimization model using measured surface a_{CDOM}.
CDOM specific absorption coefficient (λ) (normalized at 420nm)	Measured spectral a_{CDOM}.	Derived from Lee Optimization model using measured surface a_{CDOM}.
Internal Sources and Elastic Scatter		
Chlorophyll Fluorescence	Included	Included
CDOM Fluorescence	Included	Included
Raman Scattering	Included	Included
Wavelength/Bandwidth	395-705 nm / 10 nm	395-705 nm /10 nm
Wind Speed	0.25 m/s	1.0 m/s
Sky Model	Semi-Empirical	Semi-Empirical
Solar Zenith Angle	51.8^o	53.2^o
Cloud Cover	100%	25%
Downwelling Sky Irradiance	RADTRAN	RADTRAN
Bottom Boundary Condition	Finite Depth	Finite Depth
Bottom Reflectance	Independent of Wavelength (15%)	Independent of Wavelength (15%)
Output Depths	Every 0.1 m from 0-1 m, Every 0.5 m from 1-11 m.	Every 0.1 m from 0-1 m, Every 0.5 m from 1-8.3 m.